Author Manuscript

Author Manuscript

Author Manuscript

Author Manuscript

HHS Public Access

Author manuscript

Mol Psychiatry. Author manuscript; available in PMC 2022 July 27.

Published in final edited form as:

Mol Psychiatry. 2022 February ; 27(2): 1256–1273. doi:10.1038/s41380-021-01351-3.

A human microRNA (miR-20b-5p) modulates Alzheimer's disease pathways and neuronal function, and a specific polymorphism close to the *MIR20B* gene influences Alzheimer's biomarkers.

Ruizhi Wang[1,*], **Nipun Chopra**[1,*], **Kwangsik Nho**[2,*], **Bryan Maloney**[1], **Alexander G. Obukhov**[3], **Peter T. Nelson**[4], **Scott E. Counts**[5], **Debomoy K. Lahiri**[1,6,#]

[1]Laboratory of Molecular Neurogenetics, Department of Psychiatry, Indiana Alzheimer Disease; Research Center, Indiana University School of Medicine, Indianapolis, IN-46202, USA

[2]Radiology, Indiana University School of Medicine, Indianapolis, IN-46202, USA

[3]Anatomy, Cell Biology & Physiology, Indiana University School of Medicine, Indianapolis, IN-46202, USA

[4]Sanders-Brown Center on Aging, University of Kentucky, Kentucky Alzheimer's Disease Research Center, Lexington, KY, 40536, USA

[5]Departments of Translational Neuroscience and Family Medicine, Michigan State University, Grand Rapids, MI, USA; Michigan Alzheimer's Disease Research Center, Ann Arbor, MI, 48109, USA

[6]Department of Medical & Molecular Genetics, Indiana University School of Medicine, Indianapolis, IN, USA

Abstract

Alzheimer's disease (AD) is a progressive neurodegenerative disorder associated with cognitive decline and the most common form of age-related dementia. Amyloid-β peptide (Aβ) contributes to the etiology and progression of the disease. Aβ is derived from the amyloid-β precursor protein (APP). Multiple microRNA (miRNA) species are also implicated in AD. We report that human hsa-miR20b-5p (miR-20b) on Chromosome X may play complex roles in AD pathogenesis,

Users may view, print, copy, and download text and data-mine the content in such documents, for the purposes of academic research, subject always to the full Conditions of use: https://www.springernature.com/gp/open-research/policies/accepted-manuscript-terms

[#]Corresponding author: dlahiri@iupui.edu.
[*]NC, RW and KN contributed equally.
Present address: N. Chopra: DePauw University, Greencastle, IN 46135

Author contributions: RW and NC carried out cell culture experiments, RNA transfections, UTR-derived reporter clone and western blotting assays. RW did RNA extraction and quantification. NC performed Fura experiments. KN supplied and extracted ADNI data. AGO contributed to analysis of Fura experiments. PTN contributed brain tissue specimens. SEC contributed brain material and qRT-PCR of same. BM performed data analysis, and figure design. DKL performed study design and provided overall direction and facilities as well as manuscript writing and checking. All authors contributed to manuscript drafting, editing, and writing.

Conflict of Interest Statement. The authors declare no conflicts of interest regarding the contents of this work.

Ethical approval. All procedures were approved and overseen by the Institutional Biosafety Committee (IBC), Office of Research Compliance, Indiana University School of Medicine Indianapolis, IN, USA.

Supplementary Material: Supplementary information is available at MP's website.

Author Manuscript Author Manuscript Author Manuscript Author Manuscript

including Aβ regulation. Specifically, miR-20b mRNA levels were altered in association with disease progression in three regions of the human brain: temporal neocortex, cerebellum, and posterior cingulate cortex. In cultured human neuronal cells, miR-20b treatment interfered with calcium homeostasis, and neurite outgrowth and branchpoints. A single-nucleotide polymorphism (SNP) upstream of the *MIR20B* gene (rs13897515) associated with differences in levels of cerebrospinal fluid (CSF) $A\beta_{1-42}$ and thickness of the entorhinal cortex. We located a miR-20b binding site in the APP mRNA 3'-untranslated region (UTR), and treatment with miR-20b reduced APP levels. Network analysis of protein-protein interactions and gene coexpression revealed other important potential miR-20b targets among AD-related proteins/genes. MiR-20b, a miRNA that *downregulated* APP, was paradoxically associated with an *increased* risk for AD. However, miR-20b also reduced neurite growth and calcium influx, and the blockade of APP by siRNA likewise reduced calcium influx. As APP plays vital roles in neuronal health and does not exist solely to be the source of "pathogenic" Aβ, the molecular etiology of AD is likely to not just be a disease of "excess" but a disruption of delicate homeostasis.

Introduction

Alzheimer's disease (AD) is a progressive neurodegenerative disorder [1]. AD affects millions worldwide and prevalence is expected to increase as the population ages. Understanding the disorder requires investigation of biochemistry, genetics, epigenetics, and classical neurobiology [2]. AD has no cure and limited long-term treatments. A renewed enthusiasm has been kindled by aducanumab's recent approval by the FDA as potentially the first disease-modifying anti-amyloid treatment [3], although this approval is accompanied by serious questions regarding the FDA's decision and actual efficacy of the drug at reversing, halting, or even reducing cognitive decline [4]. Thus, the road remains open to research on biomarkers, small molecules that can penetrate the blood-brain barrier, short non-coding RNA-based treatments, and non-pharmacological strategies would open new avenues to tackle this devastating disease [5–8].

Pathologically, this disorder is characterized by the deposition of amyloid plaques [9] and tau tangles [10]. Plaque deposition is a consequence of the generation and aggregation of soluble amyloid β (Aβ) peptide. Once the Aβ peptide is generated, it can result in neuronal apoptosis via aberrant activation of plasma membrane expressed receptors, p75 neurotophin receptor (p75NTR) [11, 12] and N-methyl-D-aspartate receptor (NMDAR) [13]. An increase in deposition and a reduction in clearance of this peptide may play a key role in the disorder [14]. Aβ peptide is cleaved out of a large transmembrane amyloid precursor protein (APP) by two enzymes sequentially, β-site APP-cleaving enzyme-1 (BACE1) and the γ-secretase complex [15, 16]. In addition, a major contributor to risk of AD is the presence of the *APOE*ε4 allele on the apolipoprotein E gene (*APOE*) [17–25]. This risk is sufficiently strong and widespread that we considered it necessary to examine potential *APOE*ε4 effects on outcomes of human tissue/subject based experiments, herein.

APP is a single transmembrane protein found on both neurons and glial cells [15, 26, 27]. The protein is hypothesized to play roles in cell adhesion [28], neuroproliferation [29], neurite outgrowth [30], axonal guidance [31], and synaptogenesis [32]. Hence, the regulation of APP

Author Manuscript Author Manuscript Author Manuscript Author Manuscript

levels is important to normal homeostatic function. APP knockout mice are viable but exhibit aberrant long-term potentiation (LTP), impaired locomotor activity, and reduced brain weight [33–35], thereby suggesting a necessary role in brain development, learning and behavior.

According to the amyloid cascade hypothesis [3], the elimination of amyloid plaque is expected to prevent or arrest AD progression, and therefore APP, BACE1 and γ-secretase have been identified as drug targets in the treatment of AD. Unfortunately, conventional drug therapies targeting these proteins have had limited success due to a variety of factors [3, 16, 36]. Thus, there is considerable focus on the identification of novel therapies to address the Aβ excess problem. MicroRNA (miRNA) manipulation is one such possible therapeutic strategy [37, 38].

MiRNAs are short, noncoding RNA (ncRNA) that regulate the expression of many proteins at the post-transcriptional level by primarily targeting the 3' untranslated region (UTR) [38]. The seed-sequence based binding of miRNA to its cognate targets results in the reduction of protein expression due to either mRNA degradation or the inhibition of protein translation due to interference with ribosome assembly. In the case of APP, miRNAs can target either the 3' UTR or the 5' UTR, subsequently modulating protein levels [39–43]. Levels of miRNAs also differ between post-mortem brains obtained from AD patients vs. non-cognitively impaired controls. Therefore, miRNA targeting of amyloid metabolism may affect the onset and progression of AD and may constitute an important therapeutic strategy.

A focus of the present study is human hsa-miR20b-5p (miR-20b). Human miR-20b belongs to a cluster of the *MIR17* gene family that is highly conserved in vertebrates and negatively regulates APP expression [44–46]. The *MIR17* gene family consists of three paralogous groups located on chromosomes 7, 13 and X. Another member of the miR-17 family, miR-20a, is a negative regulator of APP expression [44–46]. This miRNA is 91% homologous to miR-20b-5p and their seed sequences of both are identical, yet their precursor and mature sequences are different and their chromosomal locations are different. [47]. In addition, we have been studying other important miRNAs regulating specific targets, such as BACE1, MME, and REST in primary human brain cultures and volunteer subjects with amnestic mild cognitive impairment (aMCI) [48–53].

In the present report, we identify miR-20b as a negative regulator of APP in human cell lines and a primary human cell culture model. We further show that miR-20b is present in post-mortem AD brains and the levels detected are associated with AD risk. We also demonstrate that miR-20b's reduction of APP expression is reversed by the addition of an antagomiR to miR-20b. Furthermore, we report that miR-20b can disrupt calcium homeostasis, neurite outgrowth and neuronal branchpoints in a primary human cell culture model. Finally, we identify a SNP nearby the *MIR20B* gene that is associated with AD-related cerebrospinal fluid (CSF) biomarker levels.

Author Manuscript Author Manuscript Author Manuscript Author Manuscript

Materials and Methods

Cell cultures.

HeLa cells, human glioblastoma astrocytoma (U373MG or U373), and human microglia (HMC3) and human neuroblastoma (SK-N-SH) cells were procured from ATCC (American Type Culture Collection), and grown in EMEM (Corning) supplemented with 10% Fetal Bovine Serum (FBS) until they were ~70% confluent. After a brief trypsin digestion, cells were counted using the trypan-blue exclusion method. About 150 000 cells per well were seeded in a 24-well plate and left undisturbed overnight until the transfection experiment was performed.

Primary human mixed brain cultures (PHB) were grown as described previously [48]. Briefly, primary human embryonic brain tissues were obtained from the University of Washington Birth Defects Research Laboratory (Seattle), digested with trypsin, and plated in 24-well plates at a density of 150 000 cells per well. Media (neurobasal, Invitrogen) containing b27 supplement at a ratio of 1:50, Glutamax (Invitrogen) at a ratio of 1:500, and basic fibroblast growth factor (bFGF, Invitrogen) was replenished every four days until 17 days *in vitro* (DIV 17). Transfections were performed from DIV 17 to DIV 20.

APP 3’ UTR-coupled-reporter assay.

The APP 3’ UTR was inserted downstream within a dual-reporter luciferase plasmid as described previously [41]. 50 nM of miR-20b or a negative control mimics (NCM) (ThermoFisher, lyophilyzed powder) were co-transfected with the full-length, 1.2 kb, APP 3’-UTR dual-reporter luciferase plasmid into HeLa cells and the effect of the miR-20b or NCM on luciferase reporter expression was assessed using the DualGlo luciferase assay (Promega) 48-hour post-transfection.

RNA transfection.

MiR-20b (ThermoFisher) or NCM was resuspended in nuclease free water and used at a concentration of 50 nM for HeLa experiments or 100 nM for the primary human brain tissue and human glioblastoma cultures. APP siRNA was used at a concentration of 20 nM for HeLa and 50 nM for PHB culture experiments. RNAiMax (ThermoFisher) was used as the transfection reagent at 1.5 μl/well. MiR-20b antagomiRs (ThermoFisher) were used at a 100 nM dose in all experiments. Mock-transfected cells were treated with RNAiMax, but no miRNA. The transfection complexes were suspended in Opti-Mem media (ThermoFisher) and distributed 100 μl/well. The volume per well was brought up to 500 μl/well using the appropriate media. Cells were harvested at 72 hours unless described otherwise.

Cell harvesting.

At 72-hour post-transfection (or as indicated), conditioned media was collected and stored, and cells were washed with 1× PBS and lysed using 100 μL of Mammalian protein extraction reagent (M-Per, ThermoFisher) supplemented with one tablet of protease inhibitor cocktail (Roche). The cell lysate was centrifuged for 10 minutes at 15 000×g and the supernatant was collected and used for Western blotting.

Author Manuscript Author Manuscript Author Manuscript Author Manuscript

RNA extraction and quantification from HeLa cells:

For HeLa cultures both total RNA and proteins were extracted via the miRVana Paris kit (ThermoFisher) as per the manufacturer's instructions and stored at −70°C. RNA concentration and purity were measured using a Nanodrop spectrophotometer.

RNA quantification by qRT-PCR.

RNA from cell cultures was reverse transcribed with High Capacity RNA-to-cDNA kit (ThermoFisher). cDNA was subjected to real-time qPCR analysis on QuantStudio 6 Flex instrument (ThermoFisher). Relative quantification was achieved by ΔΔCt (or "fold change") normalization with the geometric means of housekeeping genes GAPDH and ACTB.

Western blotting:

An equal amount of protein from treatment samples was denatured by heating for 10 minutes at 95°C in the Laemmle sample buffer. The denatured samples were loaded onto a 10% bis-tris, 26-lane gel (BioRad) and run at 200 V for 1.2 hours. The gels were transferred onto PVDF membranes using the iBlot dry transfer system (ThermoFisher) and were blocked using 5% Milk in tris-buffered saline with Tween-20 (TBST). Primary antibodies used were as follows: anti-APP (clone 22C11; Millipore, 1:1000), anti-actin (Sigma, 1:500 000), anti-tubulin (Sigma, 1:500 000). After TBST wash, goat anti-mouse (1:3000) secondary antibody conjugated to horseradish-peroxidase was applied for 1 hour. After washing, chemiluminescence "Super Signal" reagent (Pierce) was used to visualize protein bands.

Human brain tissue specimens.

We obtained well characterized autopsied tissue samples (Table 1) from cognitively normal older adults (non-cognitively impaired/NCI), subjects with mild cognitive impairment (MCI), or from subjects with AD. Three brain regions were examined, specifically: temporal lobe (TL, superior and middle temporal gyri, Brodmann areas 21/22) and cerebellum (CB, from lateral folia) from the University of Kentucky ADRC (P30 AG028383), and posterior cingulate cortex (PCC, Brodmann areas 23/32) from the Rush University ADRC (P30 AG010161). We recently described these tissue resources in detail [49]. Briefly, samples were frozen at autopsy and stored at −80°C. For experimental studies, samples were immersed in liquid nitrogen, powdered with a hammer, and subsequently lysed using M-Per buffer containing a protease inhibitor cocktail (Roche). After centrifugation at 13 000×g for 15 minute at 4°C, supernatants (protein lysates) were heated in Laemmli sample buffer and separated on SDS-polyacrylamide electrophoresis (PAGE).

RNA extraction from human brain tissue.

RNA was extracted from frozen tissue using a modified Ambion PureLink mini kit protocol (#12183018A). Briefly, between 10 to 25 mg of tissue was placed in a 2 ml round bottom tube. One ml of Trizol (ThermoFisher #15596026) was added. Tissue was sonicated on ice until homogenous and then allowed to incubate for 5 minutes at room temperature. Then 200 µl of chloroform was added, and the sample was vortexed for 15 seconds. Following

Author Manuscript Author Manuscript Author Manuscript Author Manuscript

a 3-minute incubation at room temperature, the samples were centrifuged at 12 000× g for 15 minutes at 4° C. The upper aqueous layer was transferred to a clean 1.5 ml tube, and an equal volume of 70% ethanol was added. The sample was vortexed and then processed following the manufacturer's instructions. RNA was eluted in a final volume of 50 μl of nuclease free water, and then quantified to be used as a template for cDNA synthesis.

MicroRNA quantification by qRT-PCR.

Quantitation of miR-20b levels was determined using two methods as described below. miR-20b levels in human tissue were analyzed by qPCR using both relative and absolute quantitative techniques. For relative quantitation, a probe-based assay for miR-20b (TaqMan 001014) was measured and compared to the control small RNA RNU48 (TaqMan 001006 labelled with VIC) [50]. Briefly, template for qPCR was generated using the TaqMan microRNA reverse transcription kit (ThermoFisher 4366596) following the manufacturer's recommended protocol with an input of 10 ng of RNA. qPCR was performed on an ABI 7500 instrument in 20 μl reactions, which were incubated for 40 amplification cycles. Each reaction contained 1.3 μl of reverse transcription product as template, 2× master mix minus uracil-N-glycosylase (UNG) (ThermoFisher 444040), and each of the TaqMan assays listed above. Ct values were determined using a constant threshold, and fold change was calculated by the delta-delta Ct method.

For absolute quantification, the TaqMan Advanced cDNA synthesis kit (ThermoFisher A28007) was used to produce template for qPCR. Ten ng of RNA was polyadenylated, ligated to an adapter, reverse transcribed, and amplified, resulting in cDNA capable of being interrogated with any TaqMan Advanced miR assay. Then qPCR amplification reactions were assembled including 2 μl of miR-AMP product as template, 2× PrimeTime master mix (Integrated DNA Technologies 1055772), and TaqMan Advanced assay miR-20b (ThermoFisher 478430) in a total of 10 μl. The reactions were subjected to 40 rounds of amplification in an ABI 7500 thermocycler. A standard curve of not less than five data points was created using known concentrations of a miR-20b synthetic oligonucleotide (IDT, Coralville, IA). Ct values were determined using a constant threshold. Construction of the standard curve was performed by creating a scatter plot in Excel based on the Ct values of the samples of synthetic miR-20b. Concentrations of unknown samples were determined by extrapolation using the slope equation generated by the standard curve.

Imaging and neurite measures.

Transfected plates (mock, miR-20b) were placed in the Incucyte® Zoom (Essen Bioscience) and imaged once a day to obtain four time points: 24, 48, 75, and-96 hours. In a separate experiment, APP siRNA treated plate was imaged at 72 hours only. Using the "neurotrack" analyzer, masking of cells and neurites were performed to ensure inclusion of cell bodies and neurites. Specifically, minimum cell body clusters were set to 50 μM^2, segmentation adjustment was set to 1.2, minimum cell width was set to 5 μM, neurite filtering was set to 'best', neurite sensitivity was set to 0.35 and the neurite width was set to 1 μM. These same parameters were used for all the conditions analyzed. The neurite lengths and branchpoints obtained were normalized to the cell body clusters (a measure of cell number within a field of view).

Author Manuscript Author Manuscript Author Manuscript Author Manuscript

Calcium imaging.

Human cells were grown on poly-D-lysine-coated coverslips (50 000 cells/well) in 35 mm dishes until DIV 17. Cells were transfected with either miR-20b or NCM for 72 hours as described above. Ratiometric, calcium sensitive fluorescent dye Fura-2 (Catalog # F1221, ThermoFisher) was used to measure intracellular calcium level changes. Cells were loaded with Fura-2 by using its acetoxymethyl (AM) ester (Fura-2AM). On DIV 20, transfected cells were washed 3× PBS and loaded for one hour with 4 μM Fura-2AM dye dissolved in 1 ml of HEPES buffered saline, followed by 3× PBS washes to remove unbound dye. Coverslips with Fura-2 loaded cells were kept in dark for 60 minutes to allow Fura-2AM to Fura-2 conversion before imaging was performed. Coverslips were placed on an inverted Zeiss microscope equipped with a back-illuminated Andor charge-coupled device camera. The coverslip was mounted into a perfusion system with continuous supply of either HEPES Buffer or HEPES buffer-containing 70 mM KCl. The coverslip was flushed with HEPES buffer for 10 minutes. During this time, regions of interest (ROI) were selected based on cell morphology; an attempt was made to include mostly non-aggregated cells. This was followed by a 5-minute application of HEPES buffer containing 70 mM KCl to depolarize the neurons. Fura-2 was excited at 350 nm and 380 nm while the emitted light was collected using a 510 nm filter. The ratio of fluorescence intensities acquired at 350 nm (F350) and 380 nm (F380) excitation wavelengths was calculated for analysis. Only cells responding to KCl were selected for analysis, as they were likely neurons.

Data for characterization of SNP in human tissues (ADNI):

Raw data used for analysis of *MIR20B* gene associated SNP effects were obtained from the Alzheimer's Disease Neuroimaging Initiative (ADNI) database (adni.loni.usc.edu). This data included serial magnetic resonance imaging (MRI), positron emission tomography (PET), biological markers, and clinical and neuropsychological assessments (Table 2).

Data Analysis.

Data was modeled for all experiments except brain level miR-20b analysis and entorhinal cortex thickness by generalized linear models (glm) followed by analysis of variance/deviance (ANOVA) and estimated marginal means using false discovery rate (fdr) to correct for multiple comparisons. A distinct advantage of the glm over ordinary least squares analysis is that the assumptions of normal distribution and similar variances (homoscedasticity) are greatly relaxed and do not need to be demonstrated for a valid analysis. Brain miRNA level data was analyzed by ordinal logistic regression (olr) followed by ANOVA. When MANOVA was used, assumptions of multivariate normality and sphericity were tested by Mardia's and Bartlett's tests, respectively. Data was found to be multivariate normal and to have homogeneous covariate matrices and was thus appropriate for MANOVA.

The olr presumes that the response variable is ordered, such as NCI, MCI, and AD representing progressive severity of condition. Since the EC data was collected using two distinct MagFields, specifically 1.5T and 3TT, we used a generalized mixed-level model with MagField as a random intercept to account for likely differences in measurements between the two settings.

Author Manuscript Author Manuscript Author Manuscript Author Manuscript

Sample sizes were determined by comparison to our earlier work, which has generated significant and repeatable results [40, 42, 54].

We calculated coefficients of determination (D) for ordinal logistic models via $D = mean(p_c) - (mean(p_c) - 1)$, where $mean(p_C)$ is the mean of each probability that corresponds to the specific level (in this case NCI/MCI/AD) reported in the data, and the second term is the remaining predicted probability sum for that point for input levels of the response variable is calculated. This method is an extension of Tjur's D for binomial logistic models [55] and is analogous to the R^2 coefficient of determination. To obtain values for each effect in the model, models were generated without an effect and D was calculated. Since D is an analogue for R^2, the Fisher transformed Z of the full model and each sub-model were calculated from $\sqrt{D}$ subtracted from transformed $\sqrt{D}$ for the overall model. The result was back-transformed and squared to produce a partial D for each effect.

Construction of interaction networks based on miR-20b and AD.

We probed the STarMirDB utility with several AD-related mRNA sequences. Positive outcomes of this search were then used as inputs to NetworkAnalyst to map minimum networks for human hippocampus protein-protein interactions (PPI), frontal cortex PPI, hippocampus co-expression, frontal cortex co-expression, and signaling pathways. Proteins/genes found in these networks were then used as input to STarMirDB to investigate further miR-20b targeting. Networks were visualized by the R "igraph" package.

Results

miR-20b alters probability of AD, MCI, and NCI in elderly adult human brain samples.

Quantitation of miR-20b in *post-mortem* samples of NCI, MCI, and AD brains (Table 1) determined a complex relationship. Raw qRT-PCR signals were quantified by both absolute (Fig. 1A–C, Table 3) and fold change (Fig. 1D–F, Table 4) methods, then analyzed with ordered logistic regression. This is an ordinal regression model—that is, a regression model for ordinal dependent variables. Ordered logistic regression can be thought of as an extension of the logistic regression model that applies to dichotomous dependent variables, allowing for more than two (ordered) response categories. Thus, just as a logistic regression can be used to predict probabilities of one of two possible outcomes, ordered logistic regression can be used to predict probabilities of each member of an ordered set of outcomes [56]. In this case, the order was NCI (no disease), MCI (mild/moderate disease), and AD (severe/worst disease).

Our model tested effects of miR-20b on diagnosis (AD/MCI/NCI) in different brain regions (temporal lobe (TL)/cerebellum (CB)/posterior cingulate cortex (PCC)). We tested potential covariates of age, sex, and presence/absence of at least one *APOE* ε4 allele. For both absolute and relative quantitation, a model that included *APOE*ε4 presence/absence as a covariate was selected. When examining absolute quantities of miR-20b, differences by miR-20b levels and *APOE*ε4 presence had significant effects (Fig. 1A–C). *APOE* ε4 presence was associated with increased probability of AD overall, as expected. As miR-20b levels increased, probability of AD increased in all three brain regions. Relative quantitation

Author Manuscript Author Manuscript Author Manuscript Author Manuscript

of miR-20b produced a model where diagnosis had no independent association with miR-20b levels (Fig. 1D–F). However, *APOE*ε4 allele presence and diagnosis significantly interacted with regard to miR-20b levels. When the *APOE* ε4 allele was absent, miR20b levels associated with reduced probability of AD and increased probability of NCI. Effects were pronounced in TL and CB samples but were very weak in PCC. Comparing fit of models by *D* (Supplemental Table 1) showed that the relative miR-20b model had greater accuracy than the absolute quantified miR-20b model. Low levels of prediction for MCI may be an artifact of the sample, which consisted primarily of NCI and AD subjects.

A single-nucleotide polymorphism (SNP) near miR-20b gene was associated with altered levels of CSF Aβ and entorhinal cortex thickness.

We queried the ADNI database for SNPs in or near the *MIR20B* gene on ChrXq26.2. One biomarker-linked SNP was identified (rs138397515). This SNP was 14.7kb upstream of *MIR20B* and consisted of an A→G transition (Fig. 2A). Out of 580 subjects (Table 2), distribution among A0/AA/G0/GA/GG genotypes was 312/229/14/24/1, where "A0" and "G0" indicate male subjects. Hardy-Weinberg χ^2 for x-linked traits determined that the alleles were within H-W equilibrium ($p = 0.775$). The "GG" genotype had only one representative and was excluded from further analysis. CSF biomarkers (CSF $A\beta_{1–42}$ and CSF p-tau) from the dataset were compared to SNP variation (Fig. 2). Analysis was carried out on the 580 subjects as a single sample group. However, SNP effects were also tested vs. potential covariates of subject age, subject education (years of attainment), subject sex, and presence of at least one *APOE*ε4 allele. Higher CSF Aβ levels were associated with the presence of at least one G allele (Fig. 2B–C. $p = 0.040$, Table 5). CSF Aβ also was associated with subject age and presence of at least one *APOE*ε4 allele ($p < 0.001$). When we examined hippocampus volume and entorhinal cortex thickness, we found no association between rs138397515 status and hippocampus volume. However, the SNP genotype did associate with differences in entorhinal cortex thickness (Fig 2 F–G; $p = 0.003$, Table 5), specifically EC thickness increased along with genotype in the order G0 < A0 < AA < GA.

miR-20b targets the APP mRNA 3' UTR activity.

Query of the hsa-miR-20b sequence against the APP 3'UTR via the StarMir algorithm [57] determined a putative site at base pairs 3158–3180 (Fig. 3A), predicted ΔG was −24.9. The site is highly conserved across multiple lineages of placental mammals, as shown by Multiz [58] alignment (Fig. 3B). We assessed the effect of miR-20b on the activity of UTR in both steady state and time course experiments. We tested an *APP* 3'-UTR luciferase reporter clone [41] by treatment with mimics for miR-20b (Fig. 3C). Treatment reduced luciferase signal vs. mock and NCM treatment ($F(df, df) = 24.136 (3, 16)$; $p < 0.001$; $\omega^2 = 0.776$).

Treatment by miR-20b alters levels of APP mRNA and protein.

Treatment of HeLa cells by miR- 20b mimics significantly reduced levels of APP mRNA (Fig. 4B), intracellular APP (Fig. 4A, C), and secreted APP (sAPP) in conditioned media (Fig. 4D). Treatment by siRNA against APP resulted in even greater reduction of these outcome measures. Co-treatment with miR-20b and an antagomiR against miR-20b prevented and reversed this response, respectively. Cell culture toxicity, as measured by LDH release, was not altered by any treatments (Fig. 4E). Of note, the NCM treatment

Author Manuscript Author Manuscript Author Manuscript Author Manuscript

significantly reduced sAPP levels. However, since this was not accompanied by reduction in APP mRNA or intracellular APP protein, this outcome may be a result of an interaction between the NCM oligomer and APP cleavage or secretion protein mRNAs. As a multivariate outcome experiment, this was analyzed by MANOVA after confirming multivariate normality by Mardia's test and sphericity by Bartlett's test. (Pillai's trace (df, df): 2.17 (5, 1); $p < 0.001$, $\eta^2 = 0.542$).

miR-20b reduced levels of APP in other human cell cultures.

We further transfected miR-20b in several additional human cell cultures, including astrocytic (U373), glial (HMC3), differentiated neuroblastoma (NBRA), and primary human brain (PHB) cultures. To explicitly test whether apparent differences in response among cell lines could be detected, we tested a model of APP ~ Treatment + Line + Treatment × Line, each blot normalized to "Mock = 1". We discovered that cell line, treatment, and the interaction of treatment and cell line/culture were significant (Table 6), indicating that apparent response differences among cell lines/cultures were also significant (Fig. 5). Treatment of miR-20b mimics reduced APP levels in U373 cells (Fig. 5A). MiR-20b treatment also significantly reduced levels of APP in HMC3 (Fig. 5B) and PHB cultures (Fig. 5C). When ATRA-differentiated neuroblastoma cultures (NBRA) were treated with mimics, APP reduction was not significant (Fig. 5D).

miR-20b and APP siRNA treatments each reduce calcium influx in a developmental human brain model culture.

We tested the effect of miR-20b and APP siRNA on calcium influx of PHB using Fura-2 imaging (Fig. 6, Table 7). An "idealized" Fura curve (Supplemental Fig. S1A), would progress through "pre-flow", from first cycle "0" to "I", which is the beginning of the influx. Influx would then progress to "P", the peak. It would then be followed by active discharge to "II", after which it would be passive tailing off. The distance from I to P, "b", is the "time to peak". The distance "b'" from P to II is the "discharge time". The height "a" is the "peak amplitude", and the height "a'" is the "ratio decay magnitude". Six comparisons were made based on different normalizations of the Fura-2 curves. Length of "pre-flow" and heights of 350/380 signal for this segment were based on raw data (Supplemental Fig. S1B). The length of "pre flow" was significantly longer for mock than for miR-20b or siRNA treated cells (Fig. 6A). However, 350/380 ratios did not significantly differ among treatments (Fig. 6B). To compare distances b, b', and a (peak height), positions of I for each treatment were normalized and trace heights were normalized to one baseline. Neither distances b (Fig. 6C) or b' (Fig. 6D) significantly differed among treatments. However, averaged peak amplitude (Fig. 6E) was significantly higher for mock-treated cells than for either miR-20b or siRNA treated cells. However, ω^2 (less-biased analog of η^2) was quite small (0.093). To compare distance a' (discharge magnitude), traces were scaled to minimum and maximum of each trace (min = 0, max = 1). No significant differences were found by treatment (Fig. 6F). In sum, while total influx was reduced by both miR-20b and APP siRNA, other elements of the process were not altered.

Author Manuscript Author Manuscript Author Manuscript Author Manuscript

miR-20b modulates neurite outgrowth and branchpoint frequency in a developmental human brain model culture.

We tested whether transfection of miR-20b modulates neuronal morphology in our PHB cultures. Both neurite branchpoints (Fig. 7A–B, Table 8) and neurite lengths (Fig. 7C–D, Table 8) were reduced over time ($p < 0.001$) when compared to Mock transfected cells, following miR-20b treatment.

Network Analysis revealed multiple potential miR-20b targets that also interact with AD-related proteins/genes.

When we constructed networks based on miR-20b targeting of AD-related mRNA sequences, we first noted that miR-20b had predicted binding sites in the mRNA sequences of multiple AD-associated gene products (Table 9). We generated 5 networks (Figs. 8–10), specifically Protein-Protein Interaction (PPI) for human hippocampus (Fig. 8A) and human frontal cortex (Fig. 8B); co-expression for human hippocampus (Fig. 9A) and human frontal cortex (Fig. 9B); and signaling pathways (Fig. 10). Upon closer examination, we found multiple hits in each network that were 1) not in the original probe list, 2) interacted with more than one AD-associated proteins, and 3) predicted to be targeted by miR-20b. What may be interesting is that none of the network types (PPI, coexpression, and signaling) overlapped for any of these discovered network members, even within the same brain region. On the other hand, within network type, there was extensive overlap for PPI between hippocampus and frontal cortex but no overlap between hippocampus and frontal cortex for coexpression. Literature search reveals that the majority of these proteins may have some function in AD, and expanding analysis of miR-20b to include these targets in AD research may be fruitful.

Discussion

Our integrated studies using different approaches, such as bioinformatics, biochemical, cellular, genetics, physiology and neuropathology, revealed potential novel roles for miR-20b in AD. We showed that miR-20b represses levels of APP by targeting a predicted 7-mer m8 on the APP 3’ UTR. This repression was seen in epithelial, astrocytic, glial, and a primary human mixed-brain cell culture model. This work adds to other reports of miRNA regulating APP levels [39–42, 44, 54, 59, 60]. Our cell culture work also showed that miR-20b reduces APP 3’-UTR activity and protein. Furthermore, we demonstrated that miR-20b and APP siRNA reduce intracellular Ca^{2+} transients in response to neuron membrane depolarization. Since our work also shows that miR-20b-5p reduces APP in glial cells, future work should address whether the miRNA can also affect intracellular calcium levels in glial cells. Treatment by miR-20b also resulted in reduction in neurite branchpoints and neurite length in human primary mixed-brain cell cultures. A SNP near *MIR20B* gene was associated with significant differences in a CSF biomarker (CSF $A\beta_{1–42}$) levels and thickness of the entorhinal cortex detected via MRI. Finally, AD progression (NCI/MCI/AD) corresponded to increases in brain miR-20b levels when miRNA was measured by pMol, and we found evidence of interaction of *APOE* ε4 allele presence and miR-20b levels.

Author Manuscript Author Manuscript Author Manuscript Author Manuscript

Our work adds knowledge about miR-20b's important role in vital cellular- and organ-level pathways. For instance, miR-20b negatively modulates many different targets including endothelial PAS domain 1 [61], vascular endothelial growth factor in the lung [62], ephrin B2 and B4 in human placental tissue [63], proteinase-activated receptor-1 [64], phosphatase and tensin homolog [65, 66], signal transducer and activator of transcription 3 [67], induced myeloid leukemia cell differentiation protein Mcl-1 [68], B-cell translocation gene [69], IL-1 receptor-associated kinase 4 [70], hypoxia-inducible factor 1-alpha [71], and protein kinase B [72].

We report that transfection of miR-20b-mediated knockdown of APP reduced both synaptic branch lengths and branchpoints in human neuronal culture. APP is expressed in the presynaptic membrane and is trafficked along via vesicles in the pre-synapse [73, 74]. Similarly, Aβ fragments are generated at both the pre-synaptic and post-synaptic neurons [75]. Previous research suggests that dimerization of APP is important to neurite growth [76], and, therefore, it is possible that our observed miR-20b effect on neurite outgrowth influences APP dimerization. It may be noteworthy that, in addition to APP and Aβ synaptic activity, BACE1 also exerts control on synaptic function [77].

The loss of synaptic integrity and function is a component of the pathologic loss of neuronal function seen in AD [78]. Maintenance of synaptic architecture is crucial to the overall brain function. Calcium-dependent vesicular-mediated neurotransmitter release is dependent on the activation of voltage-gated calcium channels in response to a depolarizing action potential traveling down the axon. However, the presence of high calcium in the cell can result in neuronal death due to excitotoxicity. The cell attempts to stabilize internal calcium levels by sequestering calcium into intracellular compartments such as the sarcoplasmic reticulum. Therefore, the cytosol and the presynaptic membrane have a low calcium concentration under normal physiological conditions.

An APP overexpression experiment could conclusively demonstrate that miR-20b alters calcium influx and neurite outgrowth via an APP pathway. However, multiple studies have already reported that APP promotes neurite outgrowth both *in vitro* and *in vivo*. For example, APP increases axonal arborization in Drosophila brains [79]. APP knockdown by shRNA inhibits neurite outgrowth in neuron cultures, while APP knockout *in vivo* reduces neurite numbers and lengths [80]. Similarly, APP regulates intracellular calcium levels. Expression of human APP in rat cortical neurons increased calcium influx [81]. Based on our data, APP siRNA and miR-20b treatment both reduce calcium influx. We can infer that miR-20b reduces calcium influx at least in part due to APP down-regulation. Nevertheless, we still must admit that we do not know whether miR-20b alters expression of other proteins independent of APP, which in turn regulate neurite outgrowth and ion channels. Future work should involve a comprehensive "-omic"-type experiment.

Small changes in the membrane expression of calcium-permeable channels can result in large-scale cellular events. These can be beneficial, for example, in the insertion of NMDAR receptors during the events of long-term potentiation. Aβ is involved in long-term potentiation (LTP) and normal memory processes [82–85], suggesting that excess removal of Aβ may impact learning. APP may itself modulate trafficking of NMDAR to the membrane

Author Manuscript Author Manuscript Author Manuscript Author Manuscript

[86]. Therefore, identifying miRNA that may influence Aβ levels would be beneficial to our understanding of Aβ's role in the synapse.

Taken together, our data suggests that increasing miR-20b levels results in loss of neuronal function, as measured by neurite length and branching, as well as a reduction in KCl-evoked intracellular calcium influx. We posit two potential mechanisms (Fig. 11). First, miR-20b reduces voltage-gated Ca^{2+} channels (VGCC) expression directly. A search of several neuronal subunits of VGCC revealed multiple potential miR-20b binding sites (supplemental Tables 2–3). Nevertheless, we speculate that the reduction observed may also be at least in part due to miR-20b reversing calcium influx by reducing APP. This may induce a subsequent reduction of available Aβ to insert into the membrane and potentially to regulate VGCC function, possibly by lowering the channel's activation threshold [87], specifically because our APP siRNA transfection induced a response that was similar to that induced by miR-20b.

We successfully measured miR-20b in post-mortem brains of NCI, MCI, and AD patients. This adds to previous work that measured miR-20b in circulating CNS-derived exosomes in the blood [88–90] as well as in peripheral tissue [91, 92]. Our work suggests levels of miR-20b differ in post-mortem brains of AD vs. NCI patients, when miR-20b is absolutely quantified. By contrast, using the ΔΔG (fold change) method resulted in no detected differences. In addition, our analysis suggests that miR-20b may increase in older individuals suffering from AD, thereby suggesting a novel interaction of changing miRNA levels with age. This observation should be investigated further. It is also important to note that our brain samples were limited to three brain regions: the posterior cingulate cortex, the cerebellar cortex, and the temporal lobe. Therefore, future studies should measure levels of miR-20b in other brain regions, such as hippocampus and entorhinal cortex.

Our data suggests that the rs138397515 (A/G) SNP, located upstream of the *MIR20B* gene on Chromosome X, is associated with increase in CSF $A\beta_{1–42}$. In addition, the SNP status was associated with differences in entorhinal cortex thickness detected by MRI. According to the ALFA project [93]. frequency of the minority "G" allele varies little among many populations (0.02 to 0.03) except among Asian populations, where the allele is not recorded and African-origin populations, where frequency is approximately 0.003 [93]. How miR-20b expression is affected by this upstream SNP will require further investigation. This SNP has the potential to participate on the complexity of effects influencing AD onset in disparate racial and ethnic groups. While apparent racial differences in AD have been reported [94], it remains unknown to what extent these differences have genetic, environmental, iatrogenic, or other unknown basis [95].

An apparent paradox underlies our present work. We demonstrated by cell culture work that application of miR-20b reduces levels of APP. However, miR-20b appears to be increased in one model relating miR-20b levels to probability of AD. Likewise, elevated levels of miR-20b appear to hamper neuronal communication (measured by neurite growth) and calcium response. Notably, the model that represented miR-20b in brain by relative quantification ($-\Delta\Delta C_T$/fold change) showed a definite *decrease* in probability of AD as miR-20b increased, and this model has a higher D (R^2 analogue) than did the model based

Author Manuscript Author Manuscript Author Manuscript Author Manuscript

on absolute quantification of miR-20b. In addition, while APP and Aβ aggregation are associated with AD pathogenesis and pathology, APP serves necessary functions, and these functions may differ in developmental vs late-life stages. For example, APP plays a vital role in neuronal pruning [96], ensuring normal development of the brain. Insufficient pruning is widely accepted as a potential cause of autism spectrum disorder [97, 98].

Taking the different outcomes and models used into account, we propose that one function of miR-20b in APP regulation is to act as a part of pruning mechanisms. APP is an adhesion protein that facilitates neurite outgrowth and proliferation at developmental stages. Suppressing such activity in a developmental model (i.e., PHB) would result in reduction in neurites and their lengths. Likewise, calcium signaling plays a vital role in neurodevelopment. The suppression of signaling by reducing APP may be a component of the pruning process (Supplemental Fig. S2). At the other end of life, in the aged individual, miR-20b downregulation of APP would help maintain lower Aβ levels, reducing excitotoxicity, aiding neuropreservation. However, if APP is de-repressed, neurodegeneration could ensue from reversing the process of blocking Aβ production (Supplemental Fig. S2C, D). Finally, our exploratory network analysis generated multiple potential novel targets connecting miR-20b regulatory activity with AD-related pathways and mechanisms. Future studies will address these pathways as well as functional interactions between miR-20b, APP, and neurodegenerative processes including Ca^{2+} dyshomeostasis and synaptic loss.

We would like to point out that we and others have noted several potential links between AD and other disorders, such as autism spectrum disorder (ASD), primarily through APP [98–101]. The present work further connects AD and ASD through APP and its metabolites and regulation, specifically in the realm of neuron growth and development.

We would be remiss were we not to provide a cautionary statement. Specifically, several conclusions are based on the use of PHB cultures. We used these cultures because they offer advantages over animal-based primary cultures (since PHB cultures are human) and over iPSC (since the PHB have not been as manipulated). In addition, they are, perforce, a mixed-cell type culture that is a better representation of human brain than is any pure cell type culture. However, this also means that the specific output of each cell type remains fully unknown, which reflects actual human brains, wherein each “pure” type of cell nevertheless is exposed, at greater or lesser levels, to other types of cells within the brain. Furthermore, PHB cultures are not genetically homogeneous but each is unique genetically and by age (of harvest). This also turns out to better resemble the reality of human populations than does a genetic monoculture. On the other hand, obtaining the stocks for human fetal brain cultures is more challenging than for traditional immortalized cell cultures or for iPSC, making it difficult to obtain sufficient power for all but the most clear-cut experimental results.

In future work, we would consider exploring larger numbers of samples, with broader age ranges (as possible), and different sources of donation, including the possibility of culturing mature brain samples [102] obtained from volunteers undergoing brain surgery. In addition, our Fura data, however apparently clear-cut, requires independent validation. Our mechanistic experiments in cell lines, PHB culture, and patient autopsy brains, would benefit

Author Manuscript Author Manuscript Author Manuscript Author Manuscript

from extension into mouse models [103–105], which would also permit testing organism effects of miR-20b modulation. We avoided mixing human and mouse systems in the present work due to potential for confounding species divergence of miRNA activity [106, 107]. This would be addressed by potentially using the mouse miR-20b or ensuring that AD-related transgene inserts included that relevant human miR-20b recognition sequences, including human 5' and 3' UTRs. We recognize that it would be tempting to do animal work in a miR-20b overexpression model, since this could potentially overcome difficulties of exogenous miR-20b administration (transient transfection). However, it would hardly be a valid model for potential treatment of AD, given that transgenic induction of miR-20b overexpression in humans would not be a practical treatment. In addition, since the familial AD types that underlie most mouse models only represent minority of human AD cases, we would also investigate inducible mouse AD models [108].

Furthermore, three clinical outcome instruments (Alzheimer's Disease Assessment Scale–Cognitive Subscale (ADAS-COG), specifically ADAS-COG 13-item [109], Mini-Mental State Examination (MMSE), [110] and Rey Auditory Verbal Learning Test (RAVLT)) [111] were administered to study participants. Relationships between these clinical scales and the rs138397515 SNP are currently under investigation.

Our present work is a first step in understanding the neurobiology of miR-20b and will propel other investigation in the near future. Our current focus was testing miR-20b's primary target at mRNA and protein levels. The majority of the field simply investigates miRNA effects on mRNA, without reference to protein output. We further presented three interaction models (protein-protein, coexpression, and signaling network). Future work would, in addition to methods mentioned, include tracing downstream and parallel pathways through RNAseq, single-cell RNA assays, and proteomics, producing a fuller picture of miR-20b's physiological roles. In a broader context, beyond miR-20b, this work should be expanded by roles of miRNA that may simultaneously function in AD and other disorders [112], influence or be influenced by currently-used drugs [7], non-pharmacological interventions, e.g., REMFS [5], and as a target or instigator of epigenetic modifications [2].

Supplementary Material

Refer to Web version on PubMed Central for supplementary material.

Acknowledgments.

The authors would like to thank Drs. Balmiki Ray and Baindu Bayon for their advice, and John Beck for technical assistance. The authors appreciate support from the Research Education and Neuroimaging Cores of the Indiana Alzheimer Disease Research Center. DKL has received grant supports from NIH-NIA (R01AG051086, R21AG4687100, and R21AG056007). KN has received grant supports from NIH (R01LM012535, R03AG054936, R03AG063250). Authors are grateful for support from the NIA IADC (P30AG010133). SEC receives grant support from NIH grants P01AG014449 (with DKL), P30AG053760, and R01AG060731.

Some data used in preparation of this article were obtained from the ADNI database (adni.loni.usc.edu). As such, investigators within ADNI contributed to the design and implementation of ADNI and/or provided data but did not participate in analysis or writing of this report. A complete listing of ADNI investigators can be found at: http://adni.loni.usc.edu/wp-content/uploads/how_to_apply/ADNI_Acknowledgement_List.pdf. ADNI--associated data collection and sharing for this project was funded by the Alzheimer's Disease Neuroimaging Initiative (ADNI) (National Institutes of Health Grant U01 AG024904) and DOD ADNI (Department of Defense award number W81XWH-12-2-0012). ADNI is funded by the National Institute on Aging, the National Institute

Author Manuscript Author Manuscript Author Manuscript Author Manuscript

of Biomedical Imaging and Bioengineering, and through generous contributions from the following: AbbVie, Alzheimer's Association; Alzheimer's Drug Discovery Foundation; Araclon Biotech; BioClinica, Inc.; Biogen; Bristol-Myers Squibb Company; CereSpir, Inc.; Cogstate; Eisai Inc.; Elan Pharmaceuticals, Inc.; Eli Lilly and Company; EuroImmun; F. Hoffmann-La Roche Ltd and its affiliated company Genentech, Inc.; Fujirebio; GE Healthcare; IXICO Ltd.; Janssen Alzheimer Immunotherapy Research & Development, LLC.; Johnson & Johnson Pharmaceutical Research & Development LLC.; Lumosity; Lundbeck; Merck & Co., Inc.; Meso Scale Diagnostics, LLC.; NeuroRx Research; Neurotrack Technologies; Novartis Pharmaceuticals Corporation; Pfizer Inc.; Piramal Imaging; Servier; Takeda Pharmaceutical Company; and Transition Therapeutics. The Canadian Institutes of Health Research is providing funds to support ADNI clinical sites in Canada. Private sector contributions are facilitated by the Foundation for the National Institutes of Health (www.fnih.org). The grantee organization is the Northern California Institute for Research and Education, and the study is coordinated by the Alzheimer's Therapeutic Research Institute at the University of Southern California. ADNI data are disseminated by the Laboratory for Neuro Imaging at the University of Southern California.

References

1. Teri L, Hughes JP, Larson EB. Cognitive deterioration in Alzheimer's disease: behavioral and health factors. J Gerontol 1990; 45(2): P58–63; doi: 10.1093/geronj/45.2.p58. [PubMed: 2313049]
2. Maloney B, Lahiri DK. Epigenetics of dementia: understanding the disease as a transformation rather than a state. Lancet Neurol 2016; 15(7): 760–774; doi: 10.1016/s1474-4422(16)00065-x. [PubMed: 27302240]
3. Selkoe DJ. Treatments for Alzheimer's disease emerge. Science 2021; 373(6555): 624–626; doi: 10.1126/science.abi6401. [PubMed: 34353940]
4. Howard R, Liu KY. Questions EMERGE as Biogen claims aducanumab turnaround. Nat Rev Neurol 2020; 16(2): 63–64; doi: 10.1038/s41582-019-0295-9. [PubMed: 31784690]
5. Perez FP, Maloney B, Chopra N, Morisaki JJ, Lahiri DK. Repeated electromagnetic field stimulation lowers amyloid-β peptide levels in primary human mixed brain tissue cultures. Sci Rep 2021; 11(1): 621; doi: 10.1038/s41598-020-77808-2. [PubMed: 33436686]
6. Ray B, Maloney B, Sambamurti K, Karnati HK, Nelson PT, Greig NH et al. Rivastigmine modifies the α-secretase pathway and potentially early Alzheimer's disease. Transl Psychiatry 2020; 10(1): 47; doi: 10.1038/s41398-020-0709-x. [PubMed: 32066688]
7. Maloney B, Balaraman Y, Liu Y, Chopra N, Edenberg HJ, Kelsoe J et al. Lithium alters expression of RNAs in a type-specific manner in differentiated human neuroblastoma neuronal cultures, including specific genes involved in Alzheimer's disease. Sci Rep 2019; 9(1): 18261; doi: 10.1038/s41598-019-54076-3. [PubMed: 31797941]
8. Perry RB, Ulitsky I. Therapy based on functional RNA elements. Science 2021; 373(6555): 623–624; doi: 10.1126/science.abj7969. [PubMed: 34353939]
9. Masters CL, Simms G, Weinman NA, Multhaup G, McDonald BL, Beyreuther K. Amyloid plaque core protein in Alzheimer disease and Down syndrome. Proc Natl Acad Sci U S A 1985; 82(12): 4245–4249; doi: [PubMed: 3159021]
10. Olsson B, Lautner R, Andreasson U, Öhrfelt A, Portelius E, Bjerke M et al. CSF and blood biomarkers for the diagnosis of Alzheimer's disease: a systematic review and meta-analysis. Lancet Neurol 2016; 15(7): 673–684; doi: 10.1016/s1474-4422(16)00070-3. [PubMed: 27068280]
11. Rabizadeh S, Bitler CM, Butcher LL, Bredesen DE. Expression of the low-affinity nerve growth factor receptor enhances beta-amyloid peptide toxicity. Proc Natl Acad Sci U S A 1994; 91(22): 10703–10706; doi: 10.1073/pnas.91.22.10703. [PubMed: 7938014]
12. Costantini C, Rossi F, Formaggio E, Bernardoni R, Cecconi D, Della-Bianca V. Characterization of the signaling pathway downstream p75 neurotrophin receptor involved in beta-amyloid peptide-dependent cell death. J Mol Neurosci 2005; 25(2): 141–156; doi: 10.1385/JMN:25:2:141. [PubMed: 15784962]
13. Shankar GM, Bloodgood BL, Townsend M, Walsh DM, Selkoe DJ, Sabatini BL. Natural oligomers of the Alzheimer amyloid-beta protein induce reversible synapse loss by modulating an NMDA-type glutamate receptor-dependent signaling pathway. J Neurosci 2007; 27(11): 2866–2875; doi: 10.1523/JNEUROSCI.4970-06.2007. [PubMed: 17360908]
14. Baranello RJ, Bharani KL, Padmaraju V, Chopra N, Lahiri DK, Greig NH et al. Amyloid-beta protein clearance and degradation (ABCD) pathways and their role in Alzheimer's disease.

Author Manuscript Author Manuscript Author Manuscript Author Manuscript

Curr Alzheimer Res 2015; 12(1): 32–46; doi: 10.2174/1567205012666141218140953. [PubMed: 25523424]

15. Haass C, Kaether C, Thinakaran G, Sisodia S. Trafficking and proteolytic processing of APP. Cold Spring Harb Perspect Med 2012; 2(5): a006270; doi: 10.1101/cshperspect.a006270.
16. Lahiri DK, Farlow MR, Sambamurti K, Greig NH, Giacobini E, Schneider LS. A critical analysis of new molecular targets and strategies for drug developments in Alzheimer's disease. Curr Drug Targets 2003; 4(2): 97–112; doi: 10.2174/1389450033346957. [PubMed: 12558063]
17. Cao J, Huang M, Guo L, Zhu L, Hou J, Zhang L et al. MicroRNA-195 rescues ApoE4-induced cognitive deficits and lysosomal defects in Alzheimer's disease pathogenesis. Mol Psychiatry 2020; doi: 10.1038/s41380-020-0824-3.
18. Lopez Lopez C, Tariot PN, Caputo A, Langbaum JB, Liu F, Riviere ME et al. The Alzheimer's Prevention Initiative Generation Program: Study design of two randomized controlled trials for individuals at risk for clinical onset of Alzheimer's disease. Alzheimer's & dementia (New York, N Y) 2019; 5: 216–227; doi: 10.1016/j.trci.2019.02.005.
19. Dafnis I, Raftopoulou C, Mountaki C, Megalou E, Zannis VI, Chroni A. ApoE isoforms and carboxyl-terminal-truncated apoE4 forms affect neuronal BACE1 levels and Abeta production independently of their cholesterol efflux capacity. Biochem J 2018; 475(10): 1839–1859; doi: 10.1042/bcj20180068. [PubMed: 29743204]
20. Rasmussen KL, Tybjaerg-Hansen A, Nordestgaard BG, Frikke-Schmidt R. Plasma levels of apolipoprotein E and risk of dementia in the general population. Ann Neurol 2015; 77(2): 301–311; doi: 10.1002/ana.24326. [PubMed: 25469919]
21. Jefferson AL, Beiser AS, Seshadri S, Wolf PA, Au R. APOE and mild cognitive impairment: the Framingham heart study. Age Ageing 2015; 44(2): 307–311; doi: 10.1093/ageing/afu183. [PubMed: 25497326]
22. Toledo JB, Da X, Weiner MW, Wolk DA, Xie SX, Arnold SE et al. CSF Apo-E levels associate with cognitive decline and MRI changes. Acta Neuropathol 2014; 127(5): 621–632; doi: 10.1007/s00401-013-1236-0. [PubMed: 24385135]
23. Verghese PB, Castellano JM, Garai K, Wang Y, Jiang H, Shah A et al. ApoE influences amyloid-beta (Abeta) clearance despite minimal apoE/Abeta association in physiological conditions. Proc Natl Acad Sci U S A 2013; 110(19): E1807–1816; doi: 10.1073/pnas.1220484110. [PubMed: 23620513]
24. Farlow MR, Lahiri DK, Poirier J, Davignon J, Schneider L, Hui SL. Treatment outcome of tacrine therapy depends on apolipoprotein genotype and gender of the subjects with Alzheimer's disease. Neurology 1998; 50(3): 669–677; doi: 10.1212/wnl.50.3.669. [PubMed: 9521254]
25. Poirier J, Delisle MC, Quirion R, Aubert I, Farlow M, Lahiri D et al. Apolipoprotein E4 allele as a predictor of cholinergic deficits and treatment outcome in Alzheimer disease. Proc Natl Acad Sci U S A 1995; 92(26): 12260–12264; doi: 10.1073/pnas.92.26.12260. [PubMed: 8618881]
26. Haass C, Hung AY, Selkoe DJ. Processing of beta-amyloid precursor protein in microglia and astrocytes favors an internal localization over constitutive secretion. J Neurosci 1991; 11(12): 3783–3793; doi: 10.1523/JNEUROSCI.11-12-03783.1991. [PubMed: 1744690]
27. LeBlanc AC, Chen HY, Autilio-Gambetti L, Gambetti P. Differential APP gene expression in rat cerebral cortex, meninges, and primary astroglial, microglial and neuronal cultures. FEBS Lett 1991; 292(1–2): 171–178; doi: 10.1016/0014-5793(91)80861-v. [PubMed: 1959603]
28. Ristori E, Cicaloni V, Salvini L, Tinti L, Tinti C, Simons M et al. Amyloid-β precursor protein APP down-regulation alters actin cytoskeleton-interacting proteins in endothelial cells. Cells 2020; 9(11); doi: 10.3390/cells9112506.
29. Caille I, Allinquant B, Dupont E, Bouillot C, Langer A, Muller U et al. Soluble form of amyloid precursor protein regulates proliferation of progenitors in the adult subventricular zone. Development 2004; 131(9): 2173–2181; doi: 10.1242/dev.01103. [PubMed: 15073156]
30. Deyts C, Vetrivel KS, Das S, Shepherd YM, Dupre DJ, Thinakaran G et al. Novel GalphaS-protein signaling associated with membrane-tethered amyloid precursor protein intracellular domain. J Neurosci 2012; 32(5): 1714–1729; doi: 10.1523/JNEUROSCI.5433-11.2012. [PubMed: 22302812]

Author Manuscript Author Manuscript Author Manuscript Author Manuscript

31. Sosa LJ, Postma NL, Estrada-Bernal A, Hanna M, Guo R, Busciglio J et al. Dosage of amyloid precursor protein affects axonal contact guidance in Down syndrome. FASEB J 2014; 28(1): 195–205; doi: 10.1096/fj.13-232686. [PubMed: 24036883]
32. Southam KA, Stennard F, Pavez C, Small DH. Knockout of amyloid β protein precursor (APP) expression alters synaptogenesis, neurite branching and axonal morphology of hippocampal neurons. Neurochem Res 2019; 44(6): 1346–1355; doi: 10.1007/s11064-018-2512-0. [PubMed: 29572646]
33. Ring S, Weyer SW, Kilian SB, Waldron E, Pietrzik CU, Filippov MA et al. The secreted beta-amyloid precursor protein ectodomain APPs alpha is sufficient to rescue the anatomical, behavioral, and electrophysiological abnormalities of APP-deficient mice. J Neurosci 2007; 27(29): 7817–7826; doi: 10.1523/JNEUROSCI.1026-07.2007. [PubMed: 17634375]
34. Phinney AL, Calhoun ME, Wolfer DP, Lipp HP, Zheng H, Jucker M. No hippocampal neuron or synaptic bouton loss in learning-impaired aged beta-amyloid precursor protein-null mice. Neuroscience 1999; 90(4): 1207–1216; doi: [PubMed: 10338291]
35. Dawson GR, Seabrook GR, Zheng H, Smith DW, Graham S, O'Dowd G et al. Age-related cognitive deficits, impaired long-term potentiation and reduction in synaptic marker density in mice lacking the beta-amyloid precursor protein. Neuroscience 1999; 90(1): 1–13; doi: [PubMed: 10188929]
36. Lahiri DK, Maloney B, Long JM, Greig NH. Lessons from a BACE1 inhibitor trial: off-site but not off base. Alzheimers Dement 2014; 10(5 Suppl): S411–419; doi: 10.1016/j.jalz.2013.11.004. [PubMed: 24530026]
37. Simion V, Nadim WD, Benedetti H, Pichon C, Morisset-Lopez S, Baril P. Pharmacomodulation of microRNA expression in neurocognitive diseases: Obstacles and future opportunities. Curr Neuropharmacol 2017; 15(2): 276–290; doi: 10.2174/1570159×14666160630210422. [PubMed: 27397479]
38. Long JM, Lahiri DK. Current drug targets for modulating Alzheimer's amyloid precursor protein: role of specific micro-RNA species. Curr Med Chem 2011; 18(22): 3314–3321; doi: 10.2174/092986711796504592. [PubMed: 21728971]
39. Long JM, Maloney B, Rogers JT, Lahiri DK. Novel upregulation of amyloid-beta precursor protein (APP) by microRNA-346 via targeting of APP mRNA 5'-untranslated region: Implications in Alzheimer's disease. Mol Psychiatry 2019; 24(3): 345–363; doi: 10.1038/s41380-018-0266-3. [PubMed: 30470799]
40. Long JM, Ray B, Lahiri DK. MicroRNA-153 physiologically inhibits expression of amyloid-beta precursor protein in cultured human fetal brain cells and is dysregulated in a subset of Alzheimer disease patients. J Biol Chem 2012; 287(37): 31298–31310; doi: 10.1074/jbc.M112.366336. [PubMed: 22733824]
41. Long JM, Lahiri DK. MicroRNA-101 downregulates Alzheimer's amyloid-beta precursor protein levels in human cell cultures and is differentially expressed. Biochem Biophys Res Commun 2011; 404(4): 889–895; doi: 10.1016/j.bbrc.2010.12.053. [PubMed: 21172309]
42. Chopra N, Wang R, Maloney B, Nho K, Beck JS, Pourshafie N et al. MicroRNA-298 reduces levels of human amyloid-β precursor protein (APP), β-site APP-converting enzyme 1 (BACE1) and specific tau protein moieties. Mol Psychiatry 2020; doi: 10.1038/s41380-019-0610-2.
43. Parsi S, Smith PY, Goupil C, Dorval V, Hebert SS. Preclinical evaluation of miR-15/107 family members as multifactorial drug targets for Alzheimer's disease. Mol Ther Nucleic Acids. 2015; 4: e256; doi: 10.1038/mtna.2015.33. [PubMed: 26440600]
44. Hebert SS, Horre K, Nicolai L, Bergmans B, Papadopoulou AS, Delacourte A et al. MicroRNA regulation of Alzheimer's Amyloid precursor protein expression. Neurobiol Dis 2009; 33(3): 422–428; doi: 10.1016/j.nbd.2008.11.009. [PubMed: 19110058]
45. Mogilyansky E, Rigoutsos I. The miR-17/92 cluster: a comprehensive update on its genomics, genetics, functions and increasingly important and numerous roles in health and disease. Cell Death Differ 2013; 20(12): 1603–1614; doi: 10.1038/cdd.2013.125. [PubMed: 24212931]
46. Tanzer A, Stadler PF. Molecular evolution of a microRNA cluster. J Mol Biol 2004; 339(2): 327–335; doi: 10.1016/j.jmb.2004.03.065. [PubMed: 15136036]

Author Manuscript Author Manuscript Author Manuscript Author Manuscript

47. Griffiths-Jones S, Grocock RJ, van Dongen S, Bateman A, Enright AJ. miRBase: microRNA sequences, targets and gene nomenclature. Nucleic Acids Res 2006; 34(Database issue): D140–144; doi: 10.1093/nar/gkj112. [PubMed: 16381832]
48. Ray B, Chopra N, Long JM, Lahiri DK. Human primary mixed brain cultures: preparation, differentiation, characterization and application to neuroscience research. Mol Brain 2014; 7: 63; doi: 10.1186/s13041-014-0063-0. [PubMed: 25223359]
49. Long JM, Ray B, Lahiri DK. MicroRNA-339–5p down-regulates protein expression of beta-site amyloid precursor protein-cleaving enzyme 1 (BACE1) in human primary brain cultures and is reduced in brain tissue specimens of Alzheimer disease subjects. J Biol Chem 2014; 289(8): 5184–5198; doi: 10.1074/jbc.M113.518241. [PubMed: 24352696]
50. Weinberg RB, Mufson EJ, Counts SE. Evidence for a neuroprotective microRNA pathway in amnestic mild cognitive impairment. Front Neurosci 2015; 9: 430; doi: 10.3389/fnins.2015.00430. [PubMed: 26594146]
51. Wang R, Maloney B, Counts SE, Lahiri DK. Alteration of a specific microRNA regulating membrane metalloendopeptidase expression in Alzheimer's disease. *Submitted* 2021; doi:
52. Wang R, Maloney B, Lahiri DK. Role of the repressor element 1 silencing transcription (REST) factor in Alzheimer's disease. 48th Annual Meeting of the Society for Neuroscience. Society for Neuroscience: San Diego, California, USA, 2018.
53. Wang R, Lahiri DK. Analyses of cell type-specific effects of microRNA-298 on native protein expression via truncated 3'-UTR hold translational promise. Sci Rep 2021; **in revision**; doi:**in revision**
54. Kumar S, Reddy PH. A new discovery of microRNA-455–3p in Alzheimer's disease. J Alzheimers Dis 2019; 72(s1): S117–s130; doi: 10.3233/jad-190583. [PubMed: 31524168]
55. Tjur T. Coefficients of determination in logistic regression models—a new proposal: the coefficient of discrimination. The American Statistician 2009; 63(4): 366–372; doi: 10.1198/tast.2009.08210.
56. Agresti A. An Introduction to Categorical Data Analysis, 3rd Edition. Wiley: Hoboken, NJ, USA, 2018, pp 159–192.
57. Kanoria S, Rennie W, Liu C, Carmack CS, Lu J, Ding Y. STarMir: tools for prediction of microRNA binding sites. Methods Mol Biol 2016; 1490: 73–82; doi: 10.1007/978-1-4939-6433-8_6. [PubMed: 27665594]
58. Blanchette M, Kent WJ, Riemer C, Elnitski L, Smit AF, Roskin KM et al. Aligning multiple genomic sequences with the threaded blockset aligner. Genome Res 2004; 14(4): 708–715; doi: 10.1101/gr.1933104. [PubMed: 15060014]
59. Liu CG, Wang JL, Li L, Wang PC. MicroRNA-384 regulates both amyloid precursor protein and beta-secretase expression and is a potential biomarker for Alzheimer's disease. Int J Mol Med 2014; 34(1): 160–166; doi: 10.3892/ijmm.2014.1780. [PubMed: 24827165]
60. Liu W, Liu C, Zhu J, Shu P, Yin B, Gong Y et al. MicroRNA-16 targets amyloid precursor protein to potentially modulate Alzheimer's-associated pathogenesis in SAMP8 mice. Neurobiol Aging 2012; 33(3): 522–534; doi: 10.1016/j.neurobiolaging.2010.04.034. [PubMed: 20619502]
61. Giraud-Triboult K, Rochon-Beaucourt C, Nissan X, Champon B, Aubert S, Pietu G. Combined mRNA and microRNA profiling reveals that miR-148a and miR-20b control human mesenchymal stem cell phenotype via EPAS1. Physiol Genomics 2011; 43(2): 77–86; doi: 10.1152/physiolgenomics.00077.2010. [PubMed: 21081659]
62. Song C, Ma H, Yao C, Tao X, Gan H. Alveolar macrophage-derived vascular endothelial growth factor contributes to allergic airway inflammation in a mouse asthma model. Scand J Immunol 2012; 75(6): 599–605; doi: 10.1111/j.1365-3083.2012.02693.x. [PubMed: 22324377]
63. Wang W, Feng L, Zhang H, Hachy S, Satohisa S, Laurent LC et al. Preeclampsia up-regulates angiogenesis-associated microRNA (i.e., miR-17, −20a, and −20b) that target ephrin-B2 and EPHB4 in human placenta. J Clin Endocrinol Metab 2012; 97(6): E1051–1059; doi: 10.1210/jc.2011-3131. [PubMed: 22438230]
64. Saleiban A, Faxalv L, Claesson K, Jonsson JI, Osman A. miR-20b regulates expression of proteinase-activated receptor-1 (PAR-1) thrombin receptor in melanoma cells. Pigment Cell Melanoma Res 2014; 27(3): 431–441; doi: 10.1111/pcmr.12217. [PubMed: 24405508]

Author Manuscript Author Manuscript Author Manuscript Author Manuscript

65. Zhu J, Chen L, Zou L, Yang P, Wu R, Mao Y et al. MiR-20b, −21, and −130b inhibit PTEN expression resulting in B7-H1 over-expression in advanced colorectal cancer. Hum Immunol 2014; 75(4): 348–353; doi: 10.1016/j.humimm.2014.01.006. [PubMed: 24468585]
66. He J, Mu M, Luo Y, Wang H, Ma H, Guo S et al. MicroRNA-20b promotes proliferation of H22 hepatocellular carcinoma cells by targeting PTEN. Oncol Lett 2019; 17(3): 2931–2936; doi: 10.3892/ol.2019.9925. [PubMed: 30854070]
67. Zhu E, Wang X, Zheng B, Wang Q, Hao J, Chen S et al. miR-20b suppresses Th17 differentiation and the pathogenesis of experimental autoimmune encephalomyelitis by targeting RORgammat and STAT3. J Immunol 2014; 192(12): 5599–5609; doi: 10.4049/jimmunol.1303488. [PubMed: 24842756]
68. Zhang D, Yi Z, Fu Y. Downregulation of miR-20b-5p facilitates Mycobacterium tuberculosis survival in RAW 264.7 macrophages via attenuating the cell apoptosis by Mcl-1 upregulation. J Cell Biochem 2019; 120(4): 5889–5896; doi: 10.1002/jcb.27874. [PubMed: 30378171]
69. Peng L, Li S, Li Y, Wan M, Fang X, Zhao Y et al. Regulation of BTG3 by microRNA-20b-5p in non-small cell lung cancer. Oncol Lett 2019; 18(1): 137–144; doi: 10.3892/ol.2019.10333. [PubMed: 31289482]
70. Tomar S, Nagarkatti M, Nagarkatti PS. 3,3'-Diindolylmethane attenuates LPS-mediated acute liver failure by regulating miRNAs to target IRAK4 and suppress Toll-like receptor signalling. Br J Pharmacol. 2015; 172(8): 2133–2147; doi: 10.1111/bph.13036. [PubMed: 25521277]
71. Liu M, Wang D, Li N. MicroRNA-20b downregulates HIF-1α and inhibits the proliferation and invasion of osteosarcoma cells. Oncol Res 2016; 23(5): 257–266; doi: 10.3727/096504016×14562725373752. [PubMed: 27098149]
72. Qin B, Liu J, Liu S, Li B, Ren J. MiR-20b targets AKT3 and modulates vascular endothelial growth factor-mediated changes in diabetic retinopathy. Acta Biochim Biophys Sin (Shanghai) 2016; doi: 10.1093/abbs/gmw065.
73. Lassek M, Weingarten J, Einsfelder U, Brendel P, Muller U, Volknandt W. Amyloid precursor proteins are constituents of the presynaptic active zone. J Neurochem 2013; 127(1): 48–56; doi: 10.1111/jnc.12358. [PubMed: 23815291]
74. Groemer TW, Thiel CS, Holt M, Riedel D, Hua Y, Huve J et al. Amyloid precursor protein is trafficked and secreted via synaptic vesicles. PLoS One 2011; 6(4): e18754; doi: 10.1371/journal.pone.0018754.
75. DeBoer SR, Dolios G, Wang R, Sisodia SS. Differential release of beta-amyloid from dendrite- versus axon-targeted APP. J Neurosci 2014; 34(37): 12313–12327; doi: 10.1523/JNEUROSCI.2255-14.2014. [PubMed: 25209273]
76. Luu L, Ciccotosto GD, Vella LJ, Cheng L, Roisman LC, Multhaup G et al. Amyloid precursor protein dimerisation reduces neurite outgrowth. Mol Neurobiol 2019; 56(1): 13–28; doi: 10.1007/s12035-018-1070-4. [PubMed: 29675574]
77. Das B, Singh N, Yao AY, Zhou J, He W, Hu X et al. BACE1 controls synaptic function through modulating release of synaptic vesicles. Mol Psychiatry 2021; doi: 10.1038/s41380-021-01166-2.
78. Selkoe DJ. Alzheimer's disease is a synaptic failure. Science 2002; 298(5594): 789–791; doi: 10.1126/science.1074069. [PubMed: 12399581]
79. Leyssen M, Ayaz D, Hébert SS, Reeve S, De Strooper B, Hassan BA. Amyloid precursor protein promotes post-developmental neurite arborization in the Drosophila brain. EMBO J 2005; 24(16): 2944–2955; doi: 10.1038/sj.emboj.7600757. [PubMed: 16052209]
80. Hoe HS, Lee KJ, Carney RS, Lee J, Markova A, Lee JY et al. Interaction of reelin with amyloid precursor protein promotes neurite outgrowth. J Neurosci 2009; 29(23): 7459–7473; doi: 10.1523/jneurosci.4872-08.2009. [PubMed: 19515914]
81. Santos SF, Pierrot N, Morel N, Gailly P, Sindic C, Octave JN. Expression of human amyloid precursor protein in rat cortical neurons inhibits calcium oscillations. J Neurosci 2009; 29(15): 4708–4718; doi: 10.1523/jneurosci.4917-08.2009. [PubMed: 19369541]
82. Bate C, Williams A. Amyloid-β(1–40) inhibits amyloid-β(1–42) induced activation of cytoplasmic phospholipase A2 and synapse degeneration. J Alzheimers Dis 2010; 21(3): 985–993; doi: 10.3233/jad-2010-100528. [PubMed: 20634578]

Author Manuscript Author Manuscript Author Manuscript Author Manuscript

83. Kim J, Onstead L, Randle S, Price R, Smithson L, Zwizinski C et al. Abeta40 inhibits amyloid deposition in vivo. J Neurosci 2007; 27(3): 627–633; doi: 10.1523/jneurosci.4849-06.2007. [PubMed: 17234594]
84. McGowan E, Pickford F, Kim J, Onstead L, Eriksen J, Yu C et al. Abeta42 is essential for parenchymal and vascular amyloid deposition in mice. Neuron 2005; 47(2): 191–199; doi: 10.1016/j.neuron.2005.06.030. [PubMed: 16039562]
85. Puzzo D, Privitera L, Fa M, Staniszewski A, Hashimoto G, Aziz F et al. Endogenous amyloid-β is necessary for hippocampal synaptic plasticity and memory. Ann Neurol 2011; 69(5): 819–830; doi: 10.1002/ana.22313. [PubMed: 21472769]
86. Cousins SL, Hoey SE, Anne Stephenson F, Perkinton MS. Amyloid precursor protein 695 associates with assembled NR2A- and NR2B-containing NMDA receptors to result in the enhancement of their cell surface delivery. J Neurochem 2009; 111(6): 1501–1513; doi: 10.1111/j.1471-4159.2009.06424.x. [PubMed: 19811606]
87. Ishii M, Hiller AJ, Pham L, McGuire MJ, Iadecola C, Wang G. Amyloid-beta modulates low-threshold activated voltage-gated l-type calcium channels of arcuate neuropeptide y neurons leading to calcium dysregulation and hypothalamic dysfunction. J Neurosci 2019; 39(44): 8816–8825; doi: 10.1523/jneurosci.0617-19.2019. [PubMed: 31537707]
88. Xiong Y, Chen L, Yan C, Zhou W, Endo Y, Liu J et al. Circulating exosomal miR-20b-5p inhibition restores wnt9b signaling and reverses diabetes-associated impaired wound healing. Small 2020; 16(3): e1904044; doi: 10.1002/smll.201904044.
89. Li M, Zhou Y, Xia T, Zhou X, Huang Z, Zhang H et al. Circulating microRNAs from the miR-106a-363 cluster on chromosome X as novel diagnostic biomarkers for breast cancer. Breast Cancer Res Treat 2018; 170(2): 257–270; doi: 10.1007/s10549-018-4757-3. [PubMed: 29557526]
90. Cochetti G, Poli G, Guelfi G, Boni A, Egidi MG, Mearini E. Different levels of serum microRNAs in prostate cancer and benign prostatic hyperplasia: evaluation of potential diagnostic and prognostic role. Onco Targets Ther 2016; 9: 7545–7553; doi: 10.2147/OTT.S119027. [PubMed: 28008272]
91. Gentile AM, Lhamyani S, Coín-Aragüez L, Clemente-Postigo M, Oliva Olivera W, Romero-Zerbo SY et al. miR-20b, miR-296, and let-7f expression in human adipose tissue is related to obesity and type 2 diabetes. Obesity (Silver Spring, Md) 2019; 27(2): 245–254; doi: 10.1002/oby.22363.
92. Katayama M, Wiklander OPB, Fritz T, Caidahl K, El-Andaloussi S, Zierath JR et al. Circulating exosomal miR-20b-5p is elevated in type 2 diabetes and could impair insulin action in human skeletal muscle. Diabetes 2019; 68(3): 515–526; doi: 10.2337/db18-0470. [PubMed: 30552111]
93. rs138397515 Refereence SNP report. https://www.ncbi.nlm.nih.gov/snp/rs138397515, 2021, Accessed 2021.
94. Babulal GM, Quiroz YT, Albensi BC, Arenaza-Urquijo E, Astell AJ, Babiloni C et al. Perspectives on ethnic and racial disparities in Alzheimer's disease and related dementias: Update and areas of immediate need. Alzheimers Dement 2019; 15(2): 292–312; doi: 10.1016/j.jalz.2018.09.009. [PubMed: 30555031]
95. Chen C, Zissimopoulos JM. Racial and ethnic differences in trends in dementia prevalence and risk factors in the United States. Alzheimers Dement (N Y) 2018; 4: 510–520; doi: 10.1016/j.trci.2018.08.009. [PubMed: 30364652]
96. Ray B, Long JM, Sokol DK, Lahiri DK. Increased secreted amyloid precursor protein-alpha (sAPPalpha) in severe autism: proposal of a specific, anabolic pathway and putative biomarker. PLoS One 2011; 6(6): e20405; doi: 10.1371/journal.pone.0020405.
97. McCaffery P, Deutsch CK. Macrocephaly and the control of brain growth in autistic disorders. Prog Neurobiol 2005; 77(1–2): 38–56; doi: 10.1016/j.pneurobio.2005.10.005. [PubMed: 16280193]
98. Sokol DK, Maloney B, Westmark CJ, Lahiri DK. Novel contribution of secreted amyloid-beta precursor protein to white matter brain enlargement in autism spectrum disorder. Front Psychiatry 2019; 10: 165; doi: 10.3389/fpsyt.2019.00165. [PubMed: 31024350]
99. Lahiri DK, Maloney B, Wang R, Sokol DK, Rogers JT, Westmark CJ. How autism and Alzheimer's disease are TrAPPed. Mol Psychiatry 2021; 26(1): 26–29; doi: 10.1038/s41380-020-00928-8. [PubMed: 33184495]

Author Manuscript Author Manuscript Author Manuscript Author Manuscript

100. Ray B, Sokol DK, Maloney B, Lahiri DK. Finding novel distinctions between the sAPPα-mediated anabolic biochemical pathways in Autism Spectrum Disorder and Fragile X Syndrome plasma and brain tissue. Sci Rep 2016; 6: 26052; doi: 10.1038/srep26052.

101. Westmark CJ, Sokol DK, Maloney B. Novel roles of amyloid-beta precursor protein metabolites in fragile X syndrome and autism. Mol Psychiatry 2016; 21(10): 1333–1341; doi: 10.1038/mp.2016.134. [PubMed: 27573877]

102. Spaethling JM, Na YJ, Lee J, Ulyanova AV, Baltuch GH, Bell TJ et al. Primary cell culture of live neurosurgically resected aged adult human brain cells and single cell transcriptomics. Cell Rep 2017; 18(3): 791–803; doi: 10.1016/j.celrep.2016.12.066. [PubMed: 28099855]

103. Hebert SS, Papadopoulou AS, Smith P, Galas MC, Planel E, Silahtaroglu AN et al. Genetic ablation of Dicer in adult forebrain neurons results in abnormal tau hyperphosphorylation and neurodegeneration. Hum Mol Genet 2010; 19(20): 3959–3969; doi: 10.1093/hmg/ddq311. [PubMed: 20660113]

104. Sasaguri H, Nilsson P, Hashimoto S, Nagata K, Saito T, De Strooper B et al. APP mouse models for Alzheimer's disease preclinical studies. EMBO J 2017; doi: 10.15252/embj.201797397.

105. Li YY, Cui JG, Hill JM, Bhattacharjee S, Zhao Y, Lukiw WJ. Increased expression of miRNA-146a in Alzheimer's disease transgenic mouse models. Neurosci Lett 2011; 487(1): 94–98; doi: 10.1016/j.neulet.2010.09.079. [PubMed: 20934487]

106. Zhang R, Peng Y, Wang W, Su B. Rapid evolution of an X-linked microRNA cluster in primates. Genome Res 2007; 17(5): 612–617; doi: 10.1101/gr.6146507. [PubMed: 17416744]

107. Cui C, Zhou Y, Cui Q. Defining the functional divergence of orthologous genes between human and mouse in the context of miRNA regulation. Brief Bioinform 2021; doi: 10.1093/bib/bbab253.

108. Melnikova T, Fromholt S, Kim H, Lee D, Xu G, Price A et al. Reversible pathologic and cognitive phenotypes in an inducible model of Alzheimer-amyloidosis. J Neurosci 2013; 33(9): 3765–3779; doi: 10.1523/jneurosci.4251-12.2013. [PubMed: 23447589]

109. Skinner J, Carvalho JO, Potter GG, Thames A, Zelinski E, Crane PK et al. The Alzheimer's Disease Assessment Scale-Cognitive-Plus (ADAS-Cog-Plus): an expansion of the ADAS-Cog to improve responsiveness in MCI. Brain Imaging Behav. 2012; 6(4): 489–501; doi: 10.1007/s11682-012-9166-3. [PubMed: 22614326]

110. Welsh-Bohmer KA, Mohs RC. Neuropsychological assessment of Alzheimer's disease. Neurology 1997; 49(3 Suppl 3): S11–13; doi: 10.1212/wnl.49.3_suppl_3.s11. [PubMed: 9310507]

111. Schmidt M. Rey Auditory Verbal Learning Test: RAVLT: a handbook. Western Psychological Association: Los Angeles, CA, USA, 1996.

112. Lahiri DK, Maloney B, Greig NH. Are pulmonary fibrosis and Alzheimer's disease linked? Shared dysregulation of two miRNA species and downstream pathways accompany both disorders. J Biol Chem 2017; 292(49): 20353; doi: 10.1074/jbc.L117.000502.

Author Manuscript Author Manuscript Author Manuscript Author Manuscript

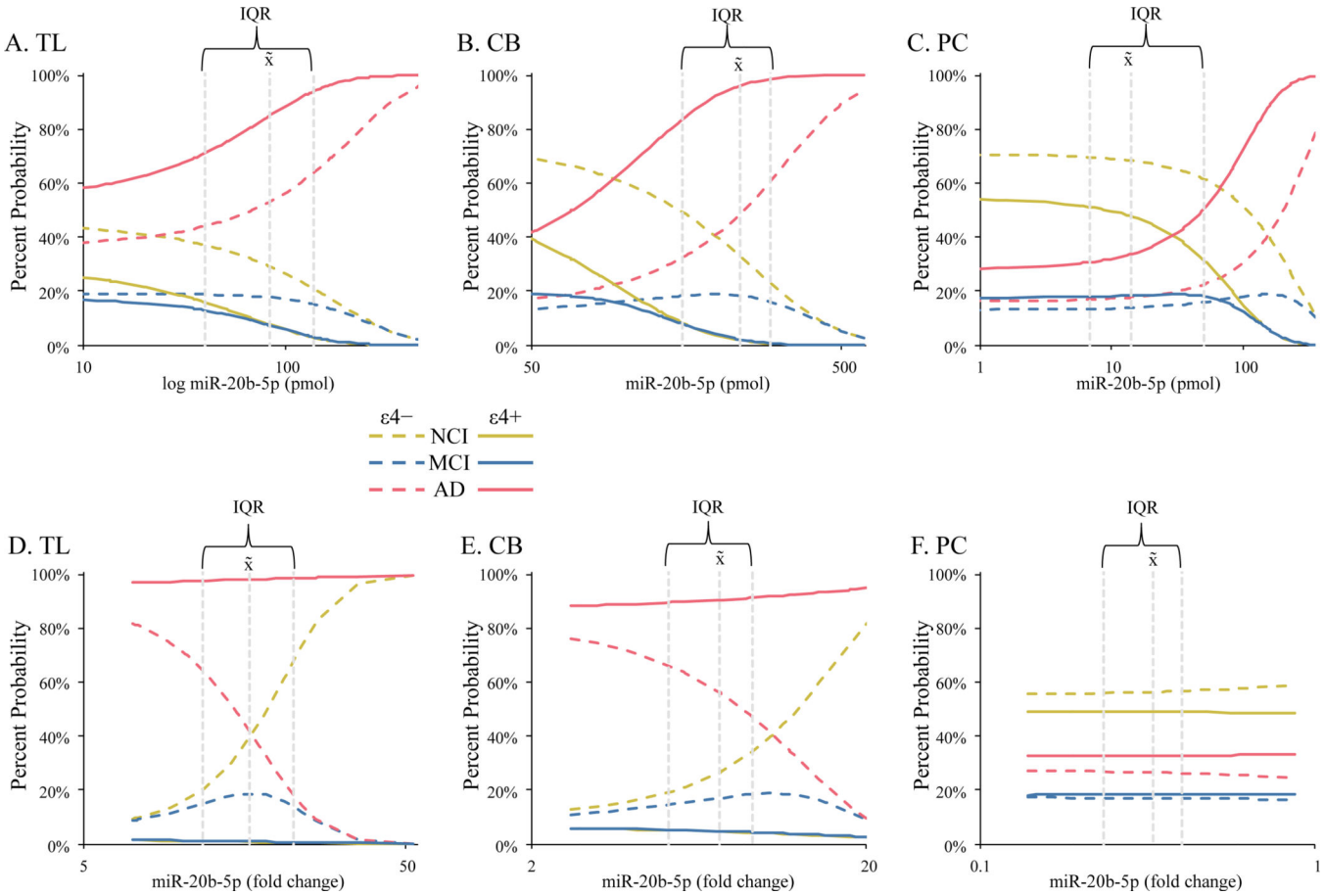


Fig. 1. Levels of miR-20b by qRT-PCR in brain autopsy samples alter probability of NCI, MCI, and AD.

miR-20b was quantified in temporal lobe (TL), cerebellum (CB), and posterior cingulate cortex (PCC) samples as described in the main text. Effect of miR-20b levels on probability of diagnosis (NCI/MCI/AD) was then modeled. **A-C**) Comparison of absolute quantitation by diagnosis and brain region. **D-F**) Comparison of $\Delta\Delta C_T$ (fold change) quantitation by diagnosis and brain region. Symbols indicate estimated marginal means categories. IQR: Interquartile range for miR-20b within a brain region. x̃: Median of miR-20b within a brain region. Significant effects are indicated by line colors and patterns, to wit: NCI, *APOE* ε4 absent: ; NCI, ε4 present: ; MCI, ε4 absent: ; MCI, ε4 present: ; AD, ε4 absent: ; AD, ε4 present: .

Author Manuscript Author Manuscript Author Manuscript Author Manuscript

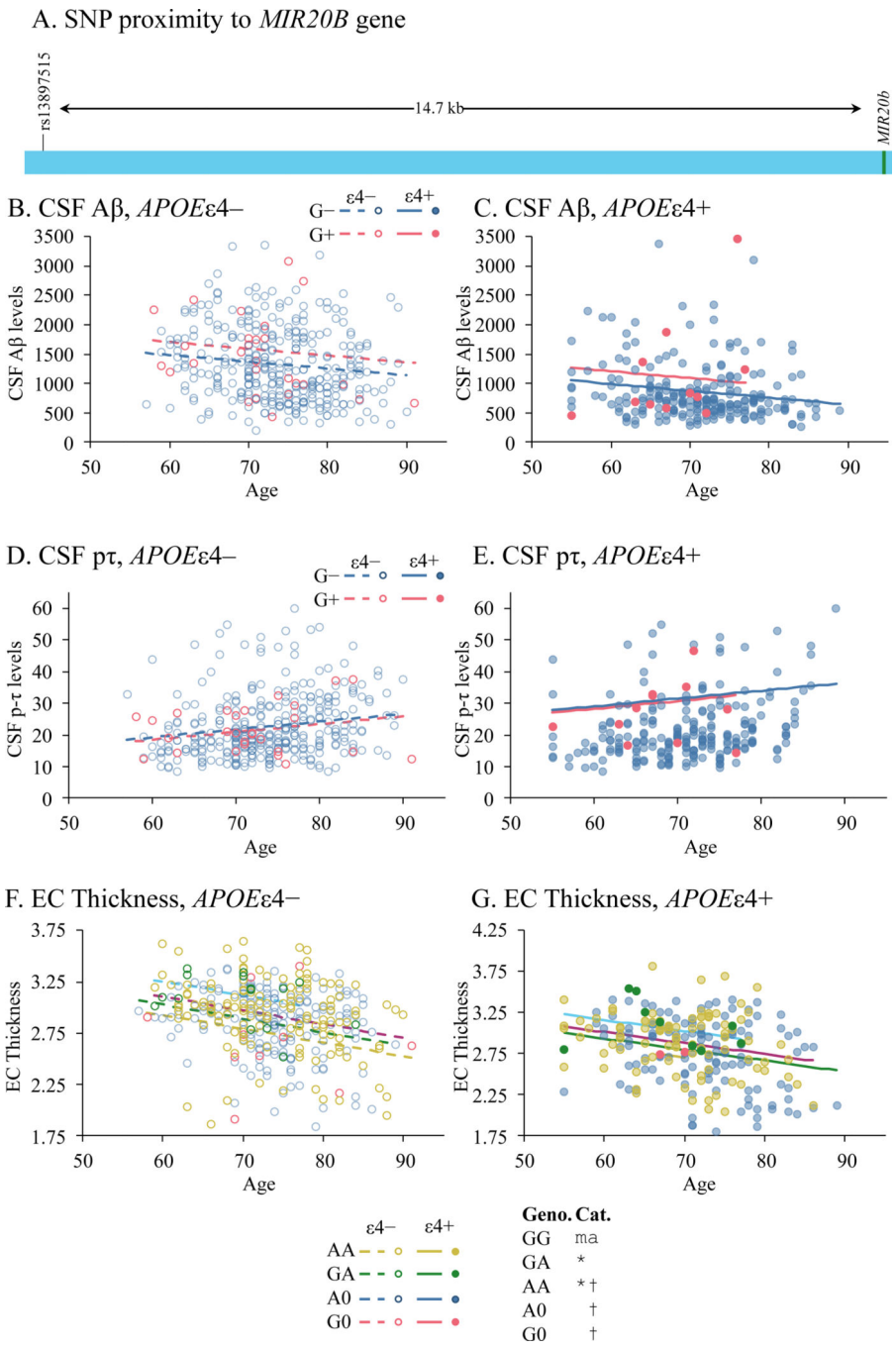
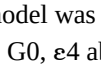
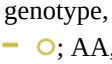


Fig. 2. The rs138397515 SNP alters levels of CSF Aβ and thickness of entorhinal cortex.

A) Location of rs13897515 relative to *MIR20B* on X chromosome. **B-C**). CSF Aβ outcomes were significantly influenced by G allele presence, age, and presence of the *APOE* ε4 allele. **D-E**) CSF p-tau (pτ) levels were significantly influenced by age and *APOE* ε4 allele presence but not by the state of the SNP. **F-G**) Thickness of the entorhinal cortex (EC) was significantly altered by SNP genotype, age and *APOE* ε4 allele presence. SNP and significant covariate effects are indicated by line/marker colors and patterns, to wit: G allele absent, *APOE* ε4 absent: – – ○; G allele present, ε4 absent: – – ○; G allele

Author Manuscript Author Manuscript Author Manuscript Author Manuscript

absent, ε4 present: ; G allele present, ε4 present: . For EC thickness, the most parsimonious model was based on genotype, with the corresponding representations: A0, ε4 absent: , G0, ε4 absent: ; AA, ε4 absent: ; GA, ε4 absent: ; A0, ε4 present: , G0, ε4 present: ; AA, ε4 present: ; GA, ε4 present: .

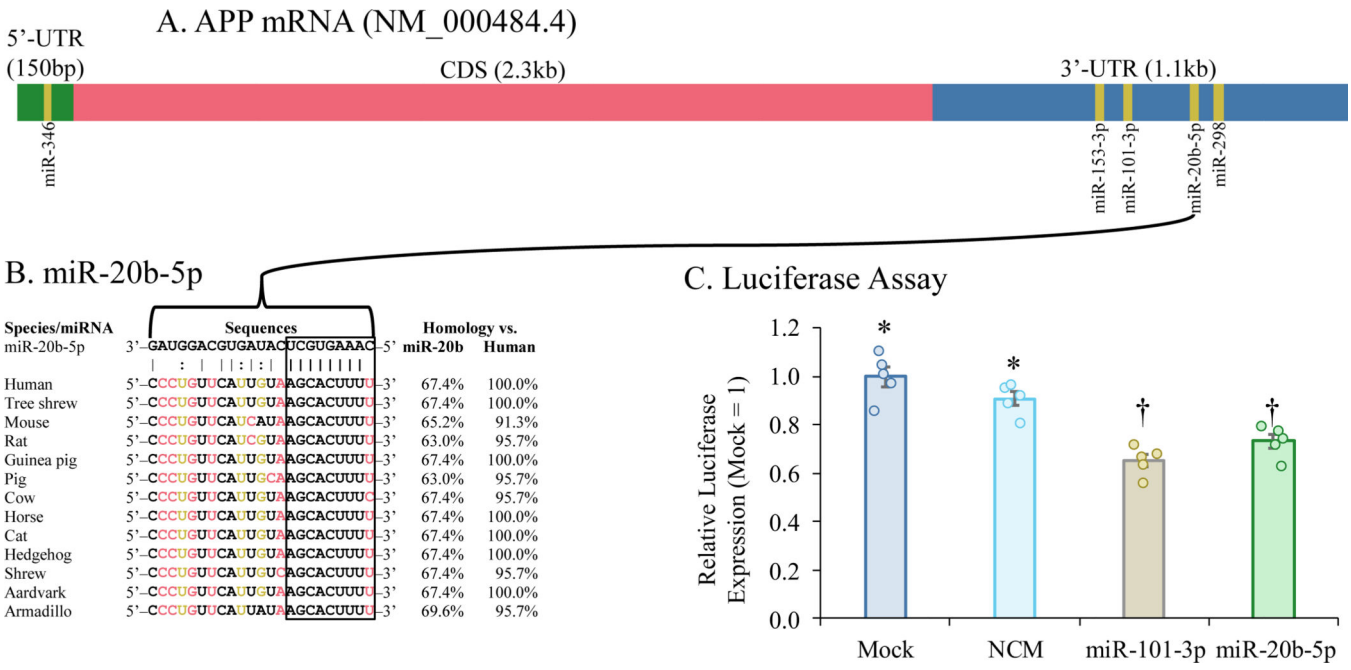


Fig. 3. MiR-20b target conservation on APP 3'-UTR and site confirmation.

A) The hsa-miR-20b sequence was used to probe the APP 3'-UTR sequence with the STarMir utility.[57] A single putative site was predicted, with 100% homology to the 8-base seed sequence. Additional miRNA species previously confirmed to regulate APP translation are also shown.[39–42] **B**) Multiple sequence alignment of homologous regions from 12 additional mammalian species. Seed sequence was conserved across multiple genera and families. Homology with human APP target sequence was >90% for all species in alignment. **C**) APP 3' UTR-coupled-reporter activity. Reporter clone with full APP 3'-UTR sequence was co-transfected with a negative control mimic (NCM), miR-101–3p, and miR-20b mimics. miR-20b significantly ($p \leq 0.05$) reduced levels of luciferase reporter expression. Symbols indicate estimated marginal means categories. Samples sharing a symbol did not significantly differ from each other. Error bars represent standard errors of means (SEM).

Author Manuscript Author Manuscript Author Manuscript Author Manuscript

Author Manuscript Author Manuscript Author Manuscript Author Manuscript

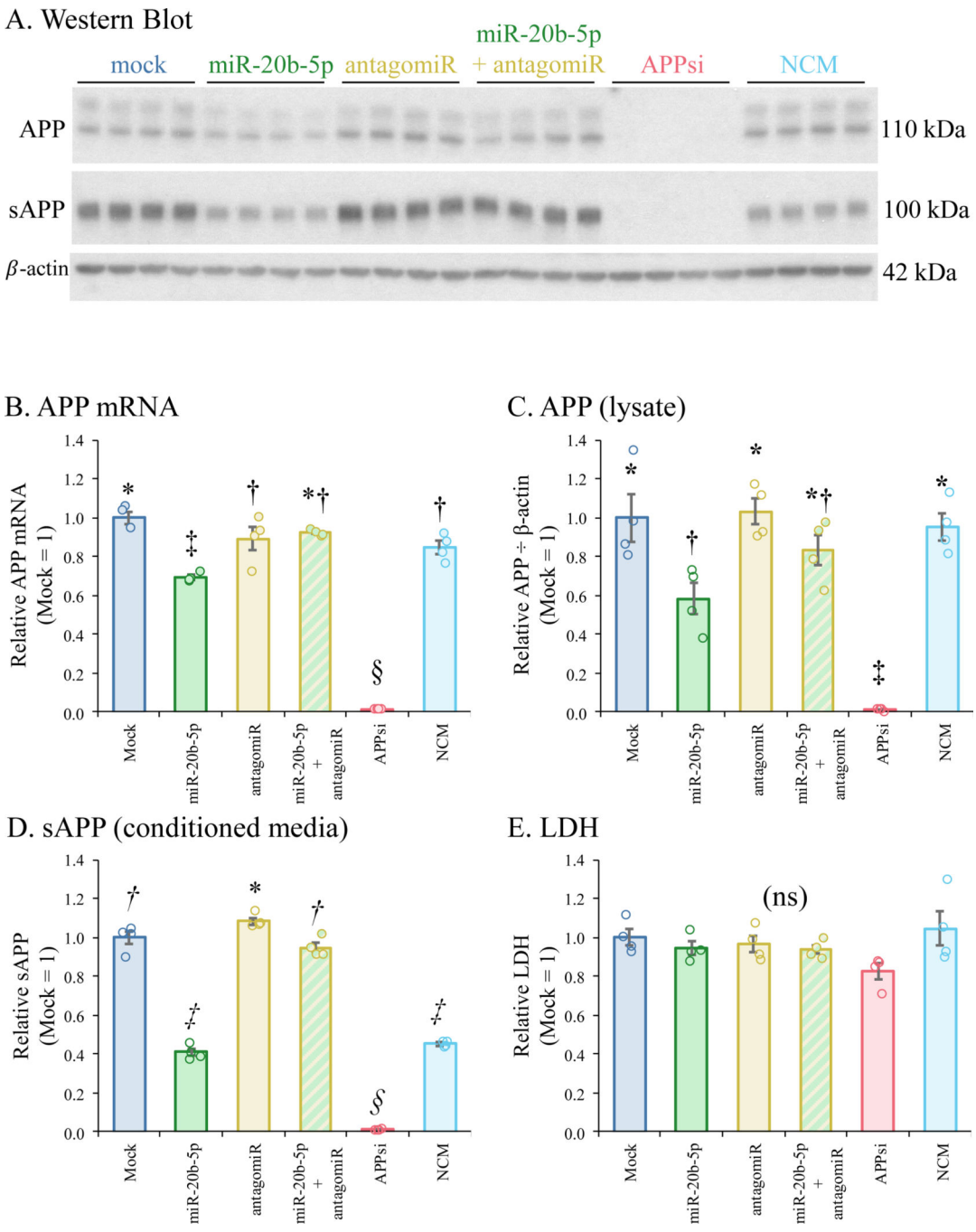


Fig. 4. Treatment with miR-20b and related oligomers produces parallel outcomes for APP mRNA, intracellular APP, and secreted APP.

HeLa cells were treated with oligomers: Specifically, miR-20b mimic, antagomiR to miR-20b, mimic + antagomiR, siRNA to APP, and a commercially obtained negative control mimic (NCM). Cultures and media were harvested and prepared for qRT-PCR and Western blotting as described in the text. LDH of cultures was also measured. Data was checked for multivariate normality then analyzed with MANOVA followed by estimated marginal means with the false discovery rate adjustment. “Pil.”: Pillai’s MANOVA trace statistic value. **A**)

Author Manuscript Author Manuscript Author Manuscript Author Manuscript

Western blot of intracellular and secreted APP (sAPP), along with β-actin. **B**) qRT-PCR relative outcomes, mock = 1. **C**) Relative densitometry of intracellular APP, mock = 1. **D**) Relative densitometry of sAPP, mock = 1. Relative LDH signal, mock = 1. Symbols indicate statistical categories. Samples sharing a symbol do not differ at $p \leq 0.05$. Error bars represent standard errors of means (SEM).

Author Manuscript
Author Manuscript
Author Manuscript
Author Manuscript

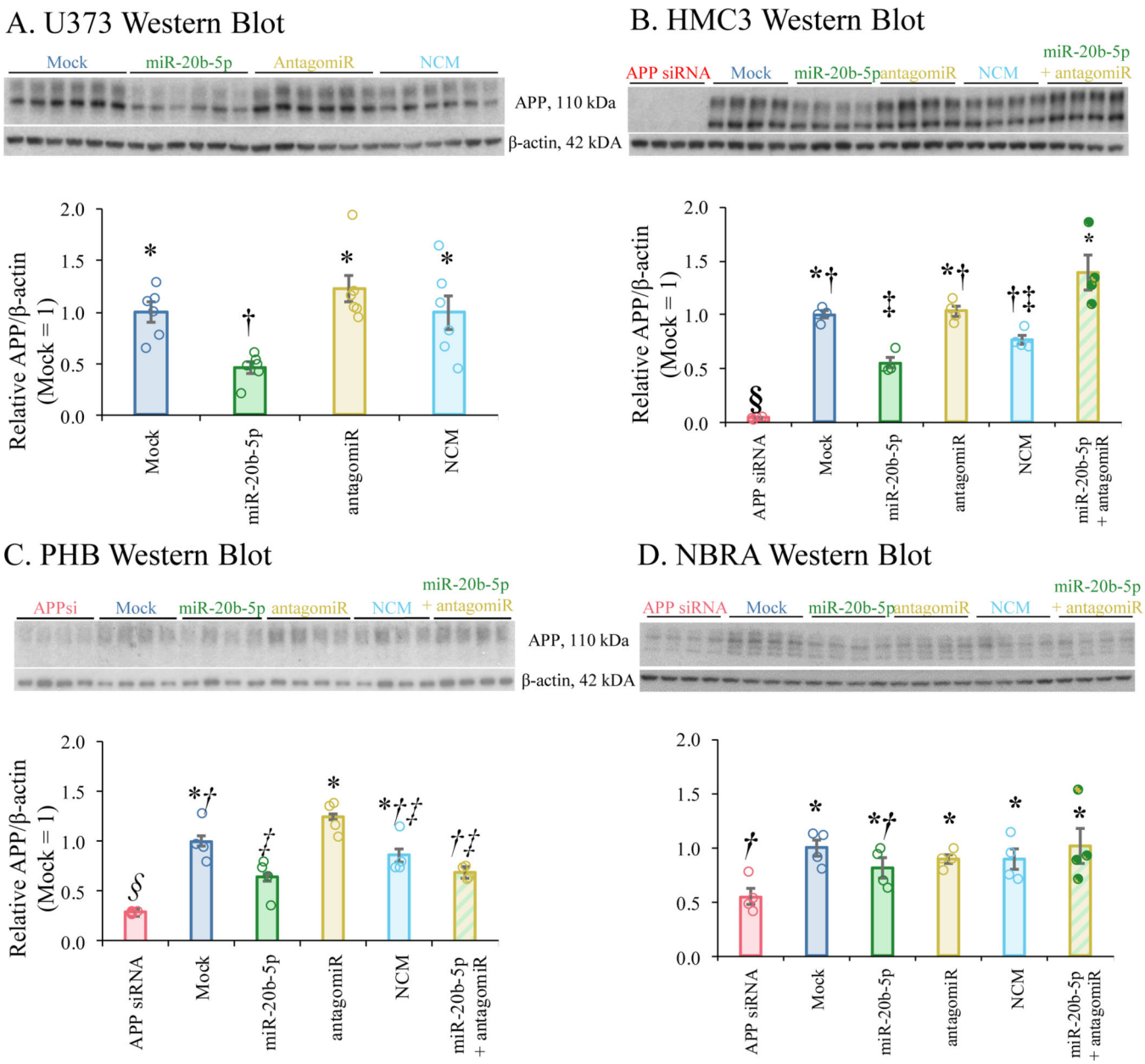


Fig. 5. Treatment with miR-20b reduced levels of APP in U373 astroglial and HeLa epithelial cells, while miR-20b reduced levels of APP in HMC3 glial cells and in human primary brain cultures (PHB) and was reversed by co-treatment with antagomiRs.

HeLa, U373, HMC3, and PHB cells were cultured and treated with different miRNA mimics or antagomiRs as specified in the main text. **A**) Western blot of APP and β-actin in HeLa. **B**) Western blotting of APP and β-actin in U373. **E**) Western blot of APP and β-actin in HMC3. **D**) By densitometry, miR-20b significantly reduced levels of APP measured by Western blot in HeLa. **E**) By densitometry, miR-20b significantly reduced levels of APP measured by Western blot in U373. **F**) By densitometry, miR-20b significantly reduced levels of APP measured by Western blot in HMC3. Co-treatment with miR-20b antagomiR eliminated this effect. **G**) Western blot of APP and β-actin in PHB. **H**) Western blot of APP and β-actin

Author Manuscript Author Manuscript Author Manuscript Author Manuscript

in NBRA. **I**) By densitometry, miR-20b reduced levels of APP measured by Western blot in PHB. Co-treatment with miR-20b antagomiR eliminated this effect. **J**) By densitometry, miR-20b did not reduce levels of APP measured by Western blot in NBRA. Co-treatment with miR-20b antagomiR had no significant effect. Symbols indicate estimated marginal means categories. Samples sharing a symbol did not significantly differ from each other. Error bars represent standard errors of means (SEM).

Author Manuscript Author Manuscript Author Manuscript Author Manuscript

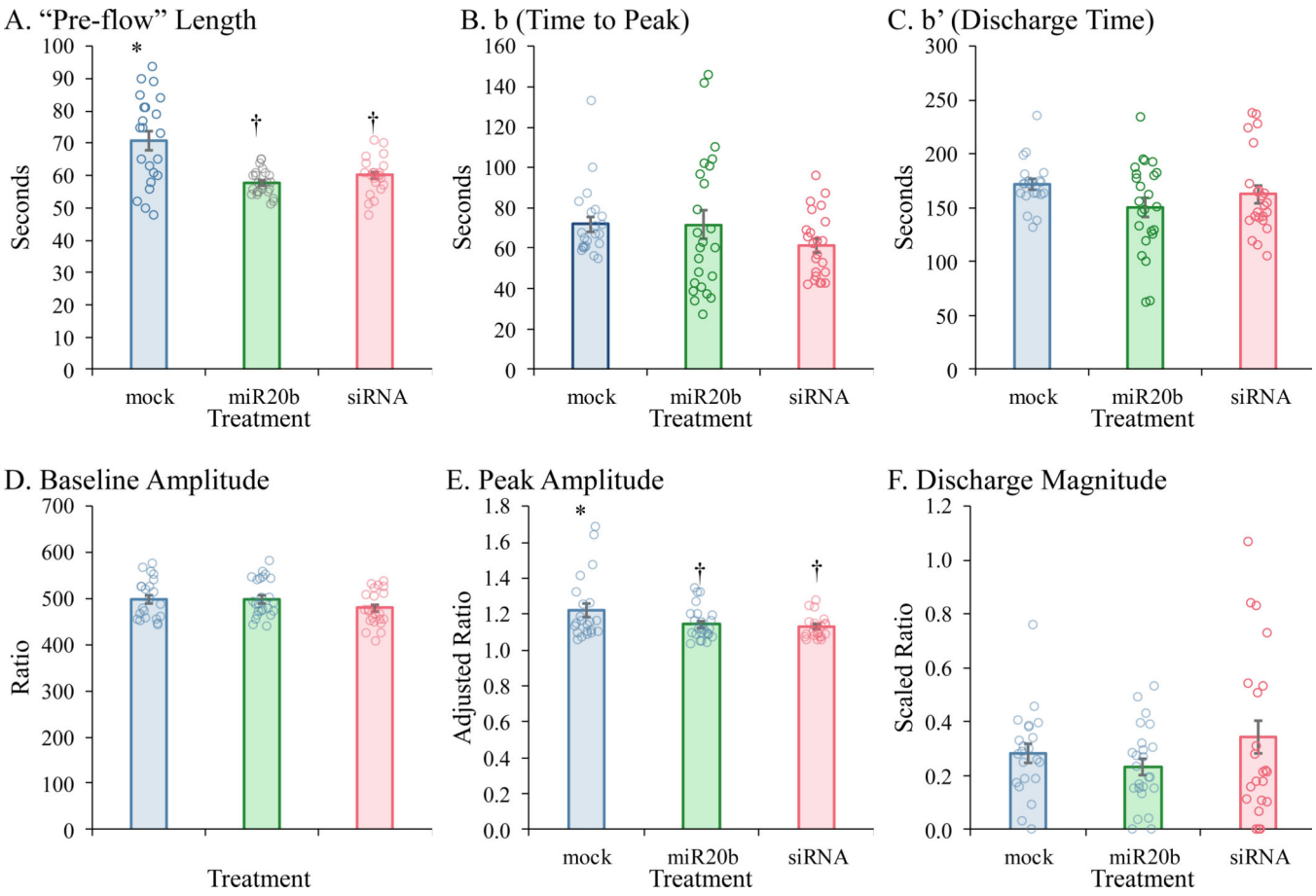


Fig. 6. Effects of miR-20b treatment on calcium efflux.

Outcomes for different measures were calculated as described in main text. **A**) "Pre-flow" length, indicating time between injection and first response. **B**) Time to peak (cycles) starting at point "0". **C**) Discharge time (between peak and "II"). **D**) Baseline ("0" to "I") amplitude. **E**) Peak amplitude. **F**) Discharge magnitude. Symbols indicate statistical groups of response over entire curve. Treatments sharing the same symbol did not significantly differ. Error bars represent standard errors of means (SEM).

Author Manuscript Author Manuscript Author Manuscript Author Manuscript

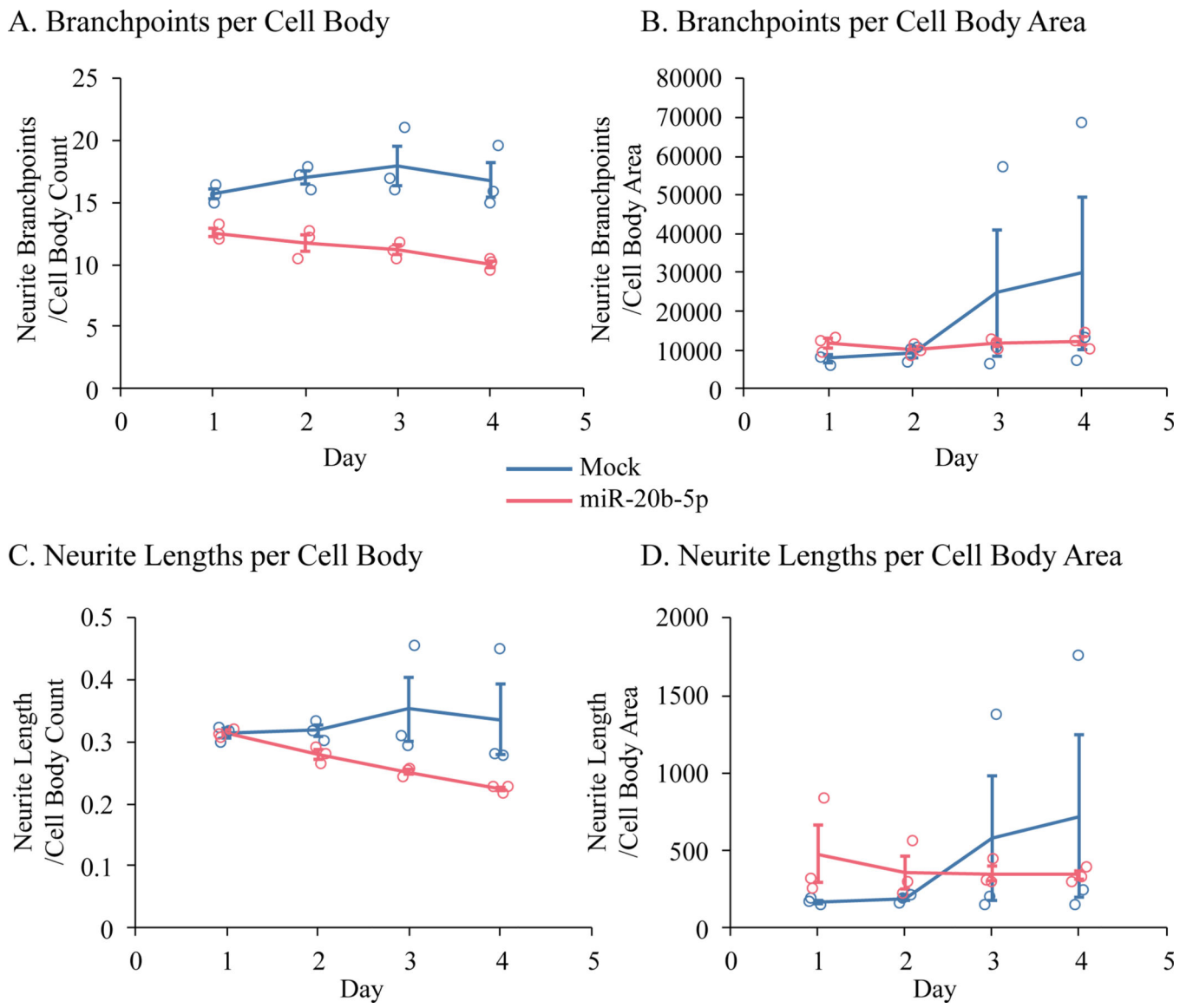
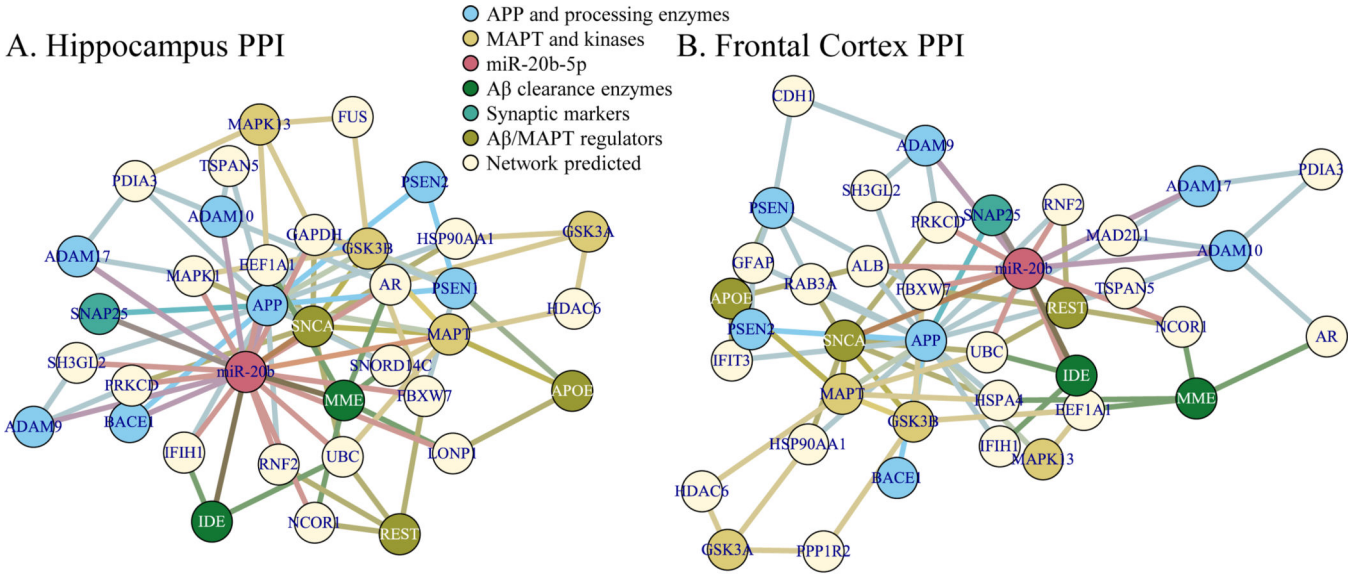


Fig. 7. Treatment with miR-20b reduced neurite branchpoints in PHB cultures.

Cells were subjected to Mock or miR-20b treatment as indicated. Neurite branchpoints were adjusted by **A**) Cell body count or **B**) Cell body area. Neurite lengths were adjusted by **C**) Cell body count or **D**) Cell body area. For both neurite branchpoints and neurite lengths, treatment with miR-20b resulted in reduced neurite branchpoints and neurite lengths, regardless of adjustment, over time vs. Mock treatment. Error bars represent standard errors of means (SEM) at each time point.

Author Manuscript Author Manuscript Author Manuscript Author Manuscript



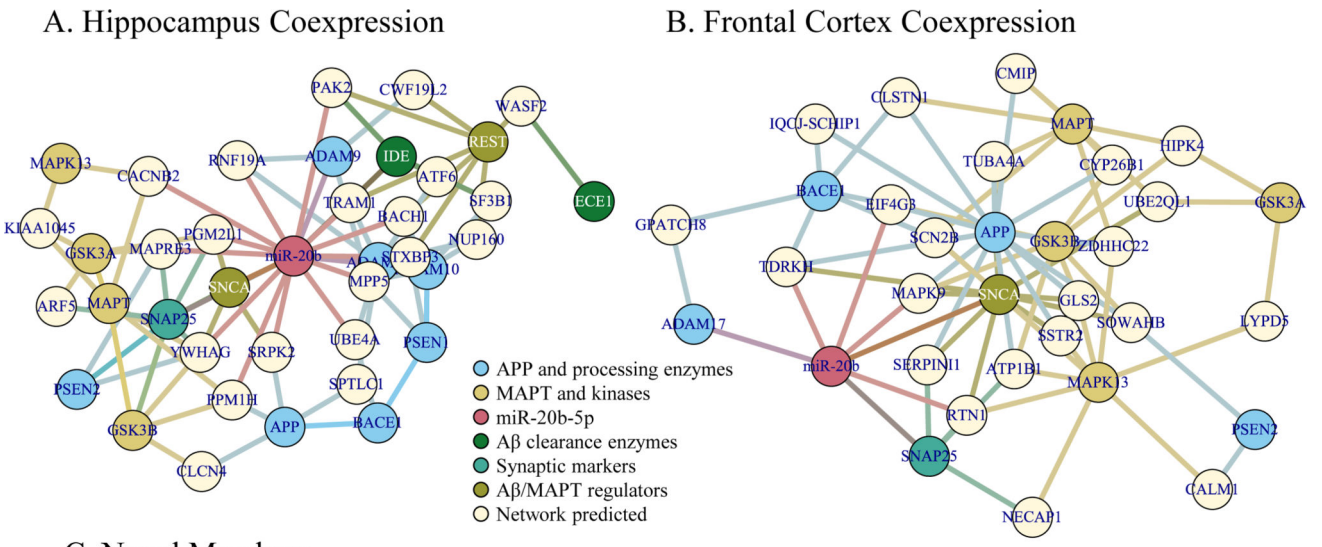
C. Novel Members

Symbol	Uniprot	Name	Protein-Protein Interaction	
			Hippocampus	Cortex
UBC	P0CG48	Polyubiquitin C precursor	miR-20b, IDE, MAPT, REST, SNCA	miR-20b, IDE, MAPT, REST, SNCA
EEF1A1	P68104	Elongation factor 1-α1	miR-20b, MAPK13, MME, SNCA	miR-20b, GSK3B, MAPK13, MME
FBXW7	Q969H0	F-box/WD repeat-containing protein 7	miR-20b, GSK3B, PSEN1, REST	miR-20b, GSK3B, PSEN1, REST
IFIH1	Q9BYX4	Interferon-induced helicase C domain-containing protein 1	miR-20b, APP, IDE	miR-20b, APP, IDE
NCOR1	O75376	Nuclear receptor corepressor 1	miR-20b, MME, REST	miR-20b, MME, REST
PRKCD	Q05655	Protein kinase C δ type	miR-20b, ADAM9, SNCA	miR-20b, ADAM9, SNCA
RNF2	Q99496	E3 ubiquitin-protein ligase RING2	miR-20b, APP, REST	miR-20b, APP, REST
MAPK1	P28482	Mitogen-activated protein kinase 1	miR-20b, ADAM17, GSK3B, SNCA	
ALB	P02768	Albumin		miR-20b, APOE, APP
CDH1	P12830	Cadherin-1		miR-20b, ADAM9, PSEN1

Fig. 8. Protein-protein interaction networks of miR-20b, AD-related targets.

Networks were generated by NetworkAnalyst as described in the text. Network nodes are color coded by protein function related to AD. **A**) Hippocampus PPI network. **B**) Frontal cortex PPI network. **C**) Summary of network members in addition to “seed” members (or “novel” members).

Author Manuscript Author Manuscript Author Manuscript Author Manuscript



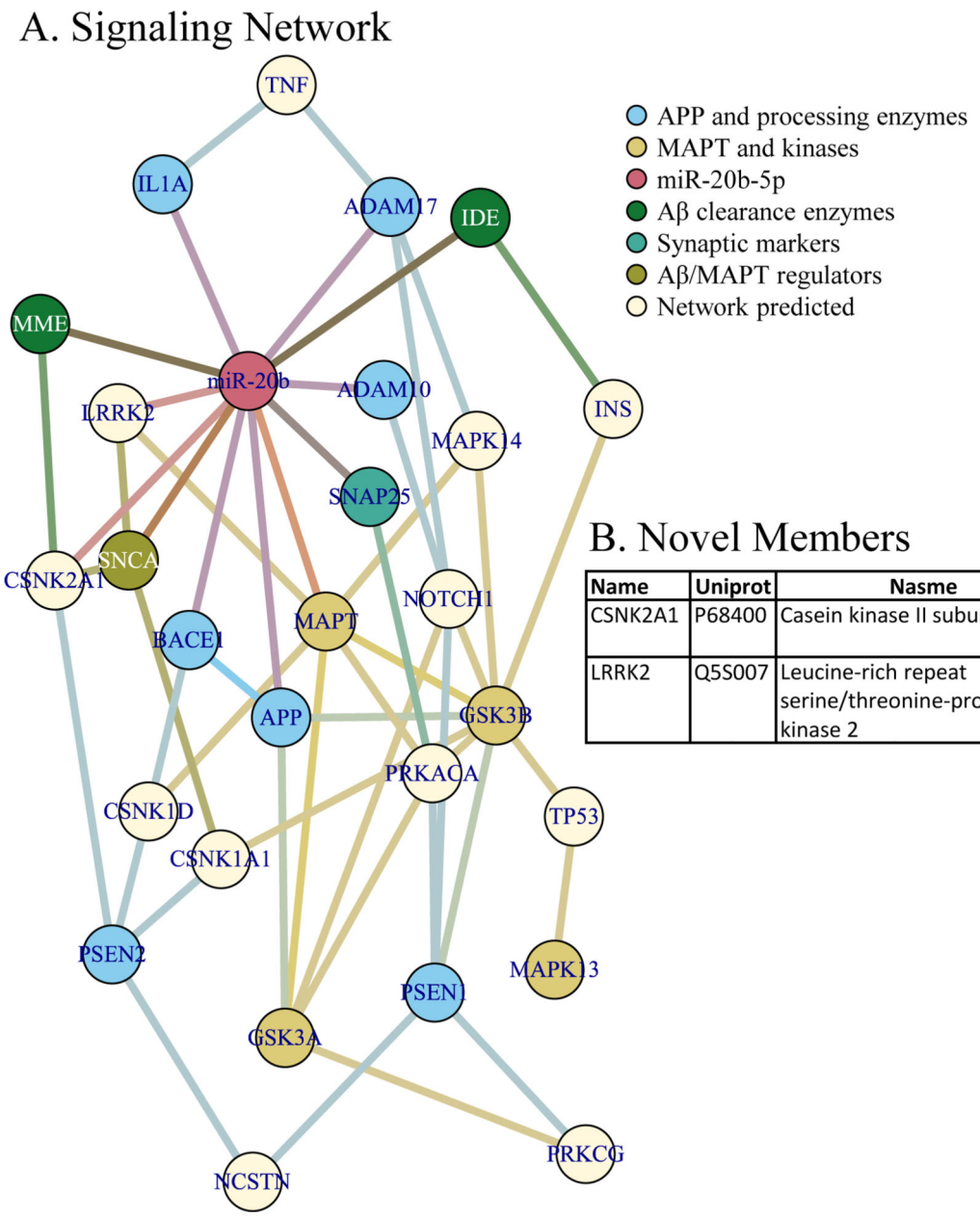
C. Novel Members

Symbol	Uniprot	Name	Coexpression	
			Hippocampus	Cortex
YWHAG	P61981	14-3-3 protein γ	miR-20b, GSK3B, MAPT, PSEN2, SNAP25, SNCA	
CLSTN1	O94985	Calsyntenin-1		miR-20b, APP, BACE1, MAPT
CYP26B1	Q9NR63	Cytochrome P450 26B1		miR-20b, APP, GSK3B, MAPT
EIF4G3	O43432	Eukaryotic translation initiation factor 4 γ 3		miR-20b, APP, BACE1, GSK3B
MAPK9	P45984	Mitogen-activated protein kinase 9		miR-20b, APP, GSK3B, SNCA
MAPRE3	Q9UPY8	Microtubule-associated protein RP/EB family member 3	miR-20b, GSK3A, PSEN2, SNAP25	
MPP5	Q8N3R9	Protein PALS1	miR-20b, ADAM10, ADAM9, PSEN1	
PGM2L1	Q6PCE3	Glucose 1,6-bisphosphate synthase	miR-20b, GSK3A, SNAP25, SNCA	
PPM1H	Q9ULR3	Protein phosphatase 1H	miR-20b, APP, GSK3B, MAPT	
RTN1	Q16799	Reticulon-1		miR-20b, MAPK13, SNAP25, SNCA
STXBP3	O00186	Syntaxin-binding protein 3	miR-20b, ADAM10, PSEN1, REST	
TDRKH	Q9Y2W6	Tudor and KH domain-containing protein		miR-20b, APP, BACE1, SNCA
BACH1	O14867	Transcription regulator protein BACH1	miR-20b, ADAM10, REST	
CACNB2	Q08289	Voltage-dependent L-type calcium channel subunit β-2	miR-20b, MAPK13, MAPT	
CALM1	P0DP23	Calmodulin-1		miR-20b, MAPK13, PSEN2
PAK2	Q13177	Serine/threonine-protein kinase PAK 2	miR-20b, IDE, REST	
RNF19A	Q9NV58	E3 ubiquitin-protein ligase RNF19A	miR-20b, ADAM17, ADAM9	
SRPK2	P78362	SRSF protein kinase 2	miR-20b, APP, SNCA	
TRAM1	Q15629	Translocating chain associated membrane protein 1	miR-20b, ADAM17, REST	
UBE4A	Q14139	Ubiquitin conjugation factor E4 A	miR-20b, ADAM17, BACE1	

Fig. 9. Coexpression networks of miR-20b, AD-related targets.

Networks were generated by NetworkAnalyst as described in the text. Network nodes are color coded by protein function related to AD. **A**) Hippocampus PPI network. **B**) Frontal cortex PPI network. **C**) Summary of network members in addition to “seed” members (or “novel” members).

Author Manuscript Author Manuscript Author Manuscript Author Manuscript



B. Novel Members

Name	Uniprot	Nasme	Signaling
CSNK2A1	P68400	Casein kinase II subunit alpha	miR-20b, MME, PSEN2, SNCA
LRRK2	Q5S007	Leucine-rich repeat serine/threonine-protein kinase 2	miR-20b, MAPT, SNCA

Fig. 10. Signaling network of miR-20b, AD-related targets.

Network was generated by NetworkAnalyst as described in the text. Network nodes are color coded by protein function related to AD. **A)** Signaling network. **B**) Summary of network members in addition to “seed” members (or “novel” members).

Author Manuscript Author Manuscript Author Manuscript Author Manuscript

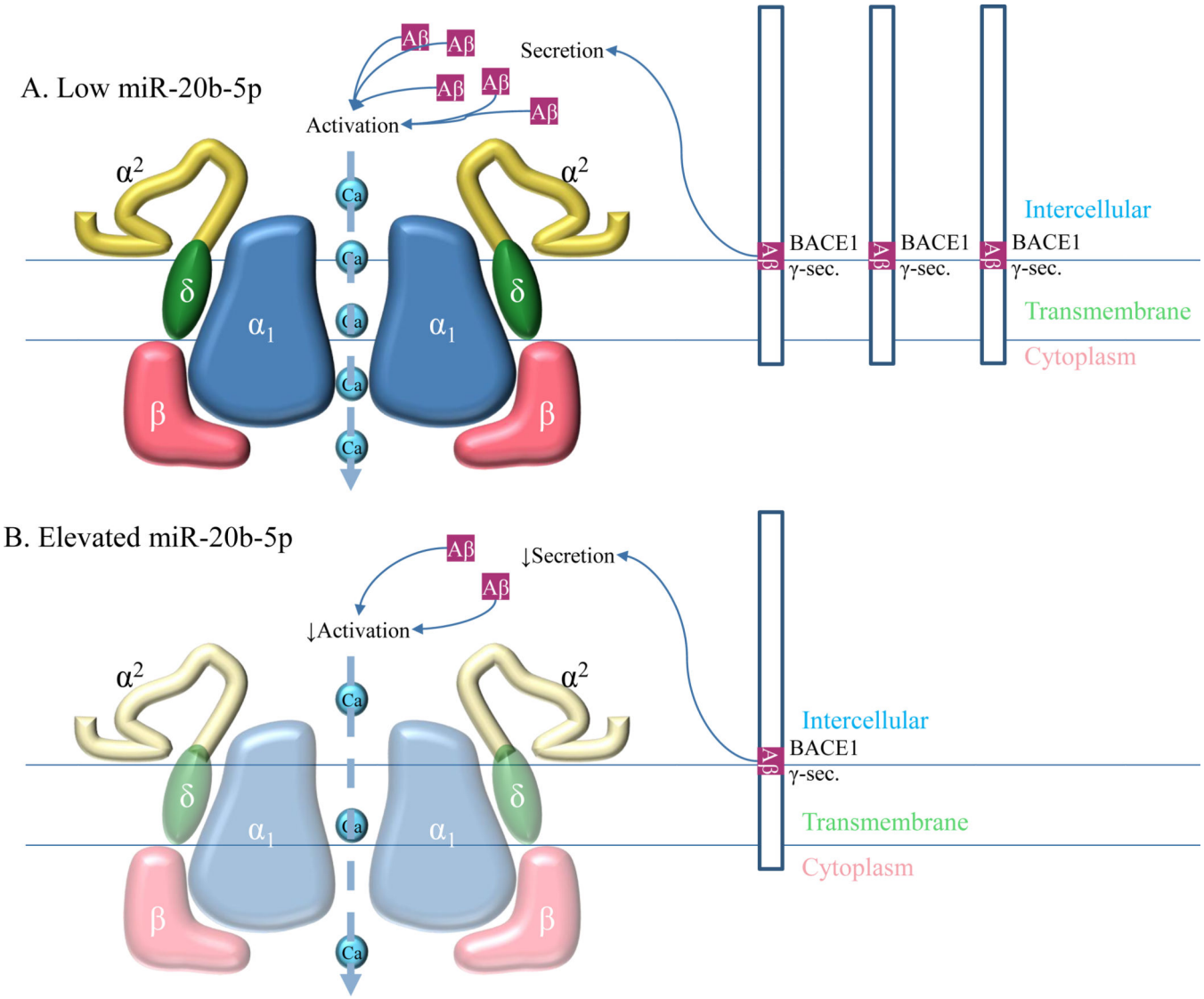


Fig. 11. Potential mechanisms of miR-20b dependent effects on calcium channel activity.

A) Under conditions of low miR-20b, subunits of VGCC are produced at higher levels, along with APP. APP is processed by BACE1 and γ-secretase complex to produce Aβ, which promotes VGCC activity, maximizing Ca influx, possibly by lowering the channel's activation threshold [87]. **B**) Under elevated miR-20b, protein translation of multiple VGCC subunits may be (partially) inhibited, reducing VGCC levels in the cell membrane. Furthermore, downregulation of APP results in reduced levels of Aβ, which decreases VGCC activity. Overall effect is reduced movement of Ca across cell membrane. Different domains of APP (right panel) are as shown: Intercellular, Transmembrane and Cytoplasmic

Author Manuscript

Author Manuscript

Author Manuscript

Author Manuscript

Table 1.

Demographics of human brain samples

Region[b]	Sex	Age (F, M)[b]
TL	12F, 10M	82.5+4.8/−2.8, 84.0+2.8/−6.8
CB	12F, 10M	82.5+4.8/−2.8, 84.0+2.8/−6.8
PC	26F, 13M	89.6+1.9/−3.8, 85.9+3.5/−3.4

[a]TL: Temporal Lobe; CB: Cerebellum; PC: Posterior Cingulate Cortex

[b]Median age in years +/− $75^{th}/25^{th}$ percentiles.

Author Manuscript

Author Manuscript

Author Manuscript

Author Manuscript

Table 2.

Demographics of ADNI SNP samples

Genotype	Number	Sex		Education[a]		Age[b]	
A0	312	0F	312 M	17	+2/−2	73.0	+5/−4
AA	229	229F	0 M	16	+2/−3	72.0	+6/−6
GA	24	24F	0 M	16	+2/−0.25	70.5	+3/−7.5
G0	14	0F	14 M	18	+0/−3.5	71.5	+5/−2.25
GG	1	1F	0 M	16	+0/−0	76.0	+0/−0

[a] Median years of formal education +/− $75^{th}/25^{th}$ percentiles.

[b] Median years of age +/− $75^{th}/25^{th}$ percentiles.

Author Manuscript

Author Manuscript

Author Manuscript

Author Manuscript

Table 3.

ANOVA of NCI/MCI/NCI vs. miR-20b levels (pmol)

Effect	χ^2 (df)	p	*D*
miR-20b	13.48 (1)	<0.001	0.021
±*APOE*ε4	9.77 (1)	0.002	0.010
Region	3.57 (2)	0.168	0.004
miR-20b × ε4	2.08 (1)	0.149	< 0.001

Author Manuscript

Author Manuscript

Author Manuscript

Author Manuscript

Table 4.

ANOVA of NCI/MCI/NCI vs. miR-20b levels (fold change)

Effect	χ^2 (df)	p	*D*
miR-20b	0.42 (1)	0.519	0.024
±*APOE*ε4	11.84 (1)	< 0.001	0.098
Region	7.09 (2)	0.029	0.144
miR-20b × ε4	11.98 (1)	< 0.001	0.039

Author Manuscript Author Manuscript Author Manuscript Author Manuscript

Table 5.

ANOVA of SNP rs138397515 status effects

Outcome	Effect	F (df, df)[a]	p	ω^2
CSF Aβ	SNP G allele ±	1.38 (1, 577)	0.040	0.005
	Age	4.42 (1, 577)	< 0.001	0.019
	*APOE*ε4 ±	32.11 (1, 577)	<0.001	0.148
CSF pτ	SNP G allele ±	0.23 (1, 577)	0.633	<0.001
	Age	14.69 (1, 577)	<0.001	0.021
	*APOE*ε4 ±	84.79 (1, 577)	<0.001	0.130
EC Thickness	Genotype[b]	14.04 (3)	0.003	).012
	Age	36.39 (1)	<0.001	0.062
	*APOE*ε4 ±	4.48 (1)	0.003	0.015

[a]Statistic for EC thickness is χ^2 (df).

[a]Genotypes in sample consist of A0, G0, AA, GA, and GG.

Author Manuscript

Author Manuscript

Author Manuscript

Author Manuscript

Table 6.

ANOVA of APP levels vs. oligomer treatments in multiple cell lines

Effect	F (df, df)	p	*D*
Treatment	6.39 (6, 90)	<0.001	0.188
Cell Line	0.32 (7, 90)	0.926	<0.001
Treatment × Line	3.15 (20, 90)	<0.001	0.214

Author Manuscript

Author Manuscript

Author Manuscript

Author Manuscript

Table 7.

ANOVA of Fura experiment outcomes

Outcome[a]	**F (df, df)**	**p**	**ω^2**
“Pre-flow” Length	16.73 (2, 66)	<0.001	0.314
b (Time to Peak)	1.41 (2, 66)	0.253	0.012
b’ (Discharge Time)	1.93 (2, 66)	0.154	0.026
Baseline Amplitude	2.33 (2, 66)	0.104	0.037
Peak Amplitude	4.53 (2, 66)	0.014	0.093
Discharge Magnitude	1.25 (2, 66)	0.294	0.007

[a]Outcomes are measured and analyzed separately.

Author Manuscript Author Manuscript Author Manuscript Author Manuscript

Table 8.

ANOVA of Fura experiment outcomes

Outcome[a]	Effect	χ^2 (df)	p	ω^2
Branchpoints per Cell Body	Treatment	29.59 (1)	<0.001	0.603
	Day	10.34 (1)	0.001	0.027
	Treatment × Day	25.07 (1)	<0.001	0.166
Branchpoints per Cell Body Area	Treatment	2.93 (1)	0.087	0.043
	Day	41.08 (1)	<0.001	0.388
	Treatment × Day	34.22 (1)	<0.001	0.282
Neurite Lengths per Cell Body	Treatment	5.87 (1)	0.015	0.111
	Day	16.24 (1)	<0.001	0.053
	Treatment × Day	33.12 (1)	<0.001	0.427
Neurite Lengths per Cell Body Area	Treatment	17.29 (1)	<0.001	0.158
	Day	22.33 (1)	<0.001	0.533
	Treatment × Day	31.77 (1)	<0.001	0.145

[a]Outcomes are measured and analyzed separately.

Author Manuscript Author Manuscript Author Manuscript Author Manuscript

Table 9.

Major AD-related proteins used as network building seeds.

Protein	Uniport	Full name	Category[a]	miR-20b[b]
ADAM10	O14672	Disintegrin and metalloproteinase domain-containing protein 10	Amyloid	+
ADAM17	P78536	Disintegrin and metalloproteinase domain-containing protein 17	Amyloid	+
ADAM9	Q13443	Disintegrin and metalloproteinase domain-containing protein 9	Amyloid	+
APOE	P02649	Apolipoprotein E	Regulator	
APP	P05067	Amyloid precursor protein	Amyloid	+
BACE1	P56817	Beta-secretase 1	Amyloid	+
ECE1	P42892	Endothelin-converting enzyme 1	Clearance	
GSK3A	P49840	Glycogen synthase kinase-3 alpha	Tau	
GSK3B	P49841	Glycogen synthase kinase-3 beta	Tau	
IDE	P14735	Insulin-degrading enzyme	Clearance	+
IL1A	P01583	Interleukin-1 alpha	Amyloid	+
IRP1	P21399	Iron-responsive element-binding protein 1	Amyloid	
IRP2	P48200	Iron-responsive element-binding protein 2	Amyloid	
MAPK13	O15264	Mitogen-activated protein kinase 13	Tau	
MAPT	P10636	Microtubule-associated protein tau	Tau	+
MME	P08473	Membrane metallo-endopeptidase	Clearance	+
PSD95	P78352	postsynaptic density protein 95	Synaptic	
PSEN1	P49768	Presenilin-1	Amyloid	
PSEN2	P49810	Presenilin-2	Amyloid	
REST	Q13127	RE1-silencing transcription factor	Regulator	
SNAP25	P60880	Synaptosomal-associated protein 25	Synaptic	+
SNCA	P37840	Alpha-synuclein	Regulator	+
SYPH	P08247	Synaptophysin	Synaptic	

[a]Classification vs. AD relationship, specifically, Amyloid: APP, APP processing enzyme, or APP translation factor; Clearance: Aβ clearing enzyme; Regulator: Protein with functions/effects on both Aβ and hyperphosphorylated tau protein; Tau: either MAPT or one of its major kinases.

[b]Predicted or confirmed to interact with miR-20b-5p